Chapter 8

Heterostructures of III-Nitride Semiconductors for Optical and Electronic Applications

Basanta Roul, Greeshma Chandan,
Shruti Mukundan and Saluru Baba Krupanidhi

Additional information is available at the end of the chapter

http://dx.doi.org/10.5772/intechopen.70219

Abstract

III-Nitride-based heterostructures are well suited for the fabrication of various optoelectronic devices such as light-emitting diodes (LEDs), laser diodes (LDs), high-power/-high-frequency field-effect transistors (FETs), and tandem solar cells because of their inherent properties. However, the heterostructures grown along polar direction are affected by the presence of internal electric field induced by the existence of intrinsic spontaneous and piezoelectric polarizations. The internal electric field is deleterious for optoelectronic devices as it causes a spatial separation of electron and hole wave functions in the quantum wells, which thereby decreases the emission efficiency. The growth of III-nitride heterostructures in nonpolar or semipolar directions is an alternative option to minimize the piezoelectric polarization. The heterostructures grown on these orientations are receiving a lot of focus due to their potential improvement on the efficiency of optoelectronic devices. In the present chapter, the growth of polar and nonpolar III-nitride heterostructures using molecular beam epitaxy (MBE) system and their characterizations are discussed. The transport properties of the III-nitride heterostructure-based Schottky junctions are also included. In addition, their applications toward UV and IR detectors are discussed.

Keywords: heterostructures, InN/GaN, InGaN/Si, InGaN/GaN, HRXRD

1. Introduction

There has been remarkable progress in the development of group III-nitride-based heterostructures because of their potential application in fabricating various optical and electronic devices such as light-emitting diodes (LEDs), laser diodes (LDs), tandem solar cells, field-effect transistors (FETs), and Schottky junctions. Heterostructures are ubiquitous of semiconductor

devices, and most of semiconductor devices have two or more semiconductor materials. A heterostructure is formed between two layers of dissimilar semiconductors having unequal energy bandgap. In order to realize high-performance devices, growth of device quality heterostructures is required. Yoshida et al. reported improved cathodoluminescence efficiency of the GaN layer grown on sapphire using AlN as a buffer layer [1]. Later Akasaki et al. [2] and Nakamura et al. [3] had employed a two-step growth method, where a nucleation layer was grown at low temperature followed by the GaN layer at high temperatures. Nakamura et al. fabricated the first blue LED consisting of a p-GaN/n-InGaN/n-GaN double heterostructure in 1993 [4] for which he won the Nobel Prize in 2014 and the first violet laser consisting of InGaN/GaN/AlGaN heterostructure in 1996 [5]. Similarly, Khan et al. [6] achieved the first breakthrough in the field of high mobility transistors based on AlGaN/GaN heterostructure in 1994.

So far most of indium gallium nitride (InGaN)-based LEDs are built along Ga-polar (0001) orientation, which is susceptible to the strong internal electric field induced by the spontaneous and the piezoelectric polarization in wurtzite III-nitrides. The effect of polarization will be explained in detail in the coming section. There have been concerted efforts in exploring III-nitride materials and devices along nonpolar and semipolar crystallographic orientations [7, 8]. The two major challenges in the field of InGaN-based LEDs are the "efficiency droop" under a high injection current density and the "green gap" in the plot of efficiency versus emission wavelength [9]. Very promising reports of LEDs and laser diodes on nonpolar and semipolar GaN bulk substrates, in the longer wavelength of green and yellow, tend to validate the concept of crystallographic engineering [10]. However, nonpolar and semipolar GaN bulk substrates are presently very small in size and expensive in price. Therefore, most of the current research in this field is focused on the growth of high-quality epilayers on nonnative substrates which are available in large wafer sizes and also cost-effective than the native substrates, thus paving the way for the commercialization of devices based on nonpolar and semipolar GaN [11]. However, the lattice mismatch along different directions poses difficulty in the hetero-epitaxial growth of nonpolar (a- and m-plane) and semipolar GaN on the foreign substrates, often resulting in nonuniform nucleation. This leads to the growth of GaN with a defective microstructure, arising due to the formation of basal-plane stacking faults (BSFs) and partial dislocations (PDs) [12, 13].

The absence of inversion symmetry in wurtzite GaN along the [0001] direction indicates that [0001] and [000−1] directions are not equivalent. Along this crystal direction if one face ends with Ga atoms, the other face will end with N atoms in the place of Ga atom and vice versa. This asymmetric arrangement of Ga and N atoms along the [0001] direction gives rise to charge polarity and thus can be referred as microscopic dipoles. The presence of polarity and lack of inversion symmetry lead to the generation of macroscopic polarization along [0001] direction and are usually referred to as spontaneous polarization. The word "spontaneous" means that it is arising only due to the crystallographic arrangement of the end faces but not due to the strain [14]. In III-nitrides, asymmetry of inversion is present only along the c-axis. Hence, P_{SP} is parallel to this direction, and c-plane nitrides are therefore called polar nitride materials. The c-axis direction consists of two opposite stacking sequences of atomic layering, resulting in either cation-face (metal) or anion-face (nitrogen) epitaxy. Ga and In polarity is in the [0001] direction, and N-polarity is in the [000−1] direction as shown in **Figure 1** [15]. The

http://dx.doi.org/10.5772/intechopen.70219

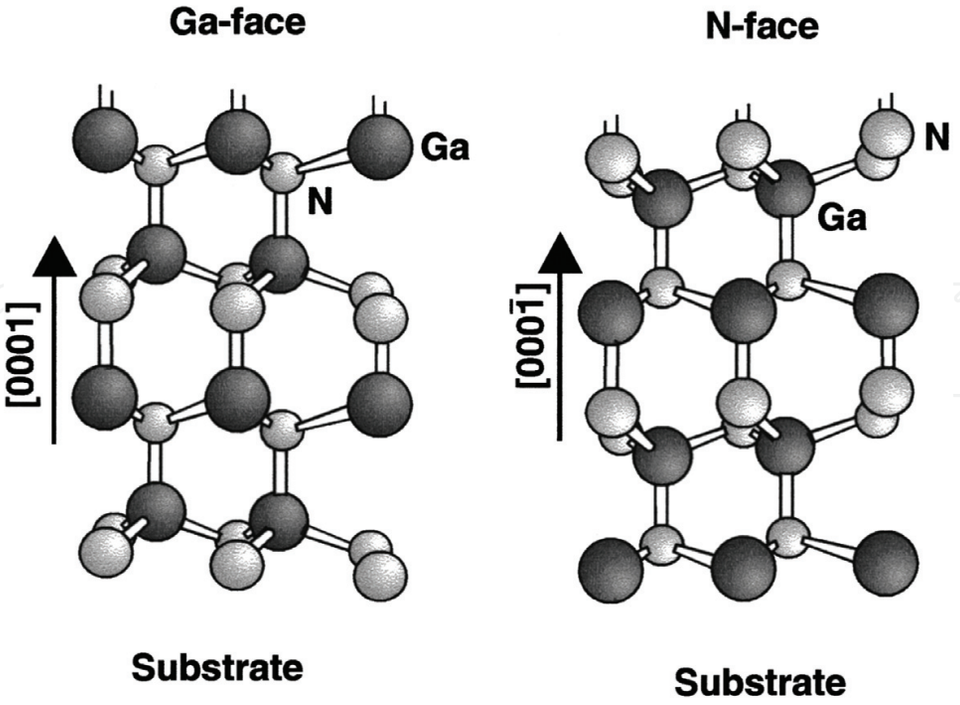

Figure 1. Ball and stick model illustrating crystal structure of wurtzite Ga-polarity and N-polarity GaN. Reprinted with permission from [15].

presence of external stress due to lattice mismatch in the films grown on foreign substrates, or in heterostructures, results in additional, piezoelectric contribution to the polarization. The total polarization, therefore, can be presented as the sum of the two components:

$$P_{total} = P_{spon} + P_{piezo} \tag{1}$$

The type of stress determines the direction of piezoelectric polarization. When a layer of smaller lattice constant than that of GaN, such as AlGaN, is grown on GaN, the grown AlGaN layer experiences tensile stress. Whereas when a layer with larger lattice constant than GaN such as InGaN is grown on GaN, the resulting strain in the InGaN layer is compressive. The piezoelectric field generated as a result of the tensile strain in the case of AlGaN/GaN and compressive strain in the case of InGaN/GaN is parallel and antiparallel, respectively. The overall polarization effect in InGaN is therefore smaller compared to AlGaN [16]. The polarization field plays a very pivotal role in GaN-based LED devices. Currently, all highly efficient blue or UV LED devices are based on multi-quantum well (MQW) structures. In a MQW structure, very few atomic layers of a narrow bandgap material, referred to as wells, are sandwiched between thicker wide bandgap materials, referred to as barriers. In quantum well (QW) structures, the charge carriers are confined to wells with high-energy barriers on either side, thus preventing the charge carriers from escaping without recombining with their counterparts and thus increasing the probability of radiative recombination. The presence of spontaneous and piezoelectric polarization in QW leads to asymmetry in the electric-field profile and results in bending of the conduction and valence bands, thus spatially separating the charge carriers. Due to this spatial separation of the charge carriers, the overlapping of charge

carrier wave functions is substantially reduced resulting in lower recombination probability. The bending of bands also leads to bandgap shrinkage. As a result the emitted radiation is red-shifted [17]. This process is referred to as quantum-confined Stark effect and is undesirable.

Apart from the above-mentioned detrimental effects, the effective width of QWs is reduced as a consequence of tilt in the band edges which leads to a higher charge carrier density and may eventually lead to nonradiative Auger recombination. The effective barrier height is also lowered due to band bending, which means the carrier confinement is weakened with increasing bias voltage leading to carrier leakage. It is believed that these two non-radiative recombination mechanisms are responsible for the reduced efficiency in GaN-based LEDs when operated at higher current [18]. Besides wurtzite nitrides, cubic nitrides also have similar bandgaps and are free from the spontaneous polarization. However, due to the instability of cubic nitrides and the poor quality, they are less preferred for device applications. Growth of wurtzite materials that have either no polarization field or reduced one in the growth direction can solve these problems. **Figure 2**(**b**–**i**) shows the wurtzite III-nitride planes which are perpendicular or inclined to the [0001] direction [19]. There are two surfaces perpendicular to the

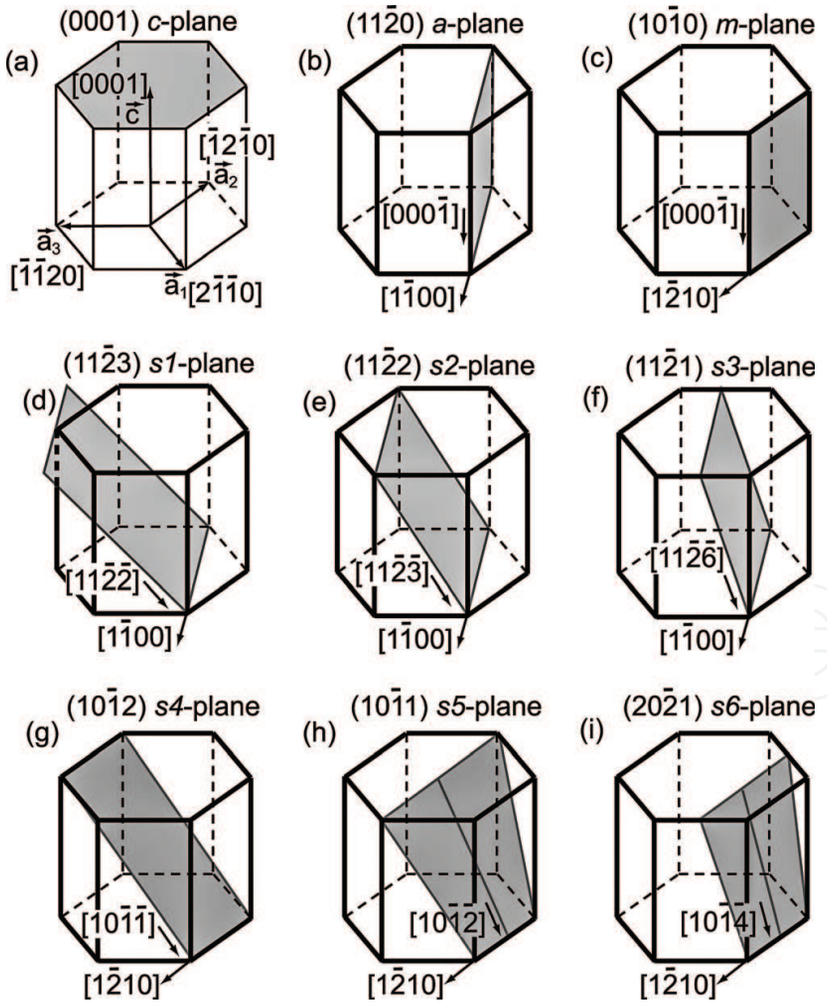

Figure 2. Schematic views of (a) polar c-plane; (b) and (c) nonpolar a- and m-planes; (d)–(i) various semipolar s-planes. Reprinted with permission from [19].

c-axis, which have equal number of Group III and V atoms and are called nonpolar surfaces. Alternatively, inclined surfaces such as (1 0 −1 −3), (1 0 −1 −1), and (1 1 −2 2) are known to have lower polarization fields and are often called semipolar planes [20].

Compared to the conventionally oriented c-plane GaN, nonpolar and semipolar planes were considered "unstable" for a long time. Rough and faceted surfaces have been a prolonged problem for device fabrication on these directions [21, 22]. In 2000, Waltereit et al. first demonstrated planer m-plane GaN growth via molecular beam epitaxy [7]. This demonstration was followed by Craven et al.'s metal organic chemical vapor deposition growth of a-plane GaN films in 2002 [23]. While considerable progress started after this breakthrough in the growth of thin films in nonpolar orientation, thick-film or bulk growth of this orientation continued to be elusive, hence limiting the performance of nonpolar GaN-based devices due to lack of suitable substrates. Achieving low defect density, nonpolar oriented film is a trending problem and exponential progress is seen in this field over the past decade. In the present chapter, the growth of polar and nonpolar III-nitride heterostructures using molecular beam epitaxy (MBE) and their characterizations will be presented. The transport properties of the III-nitride heterostructure-based Schottky junctions will be presented. In addition, applications toward UV and IR detectors will be discussed.

2. Growth and characterizations of III-nitride heterostructures

2.1. Polar InN/GaN heterostructures

The InN/GaN heterostructure system has several advantages which includes the high rate of optical phonon emission in InN (2.5×10^{13} s^{-1}), high peak value of the steady-state electron drift velocity in InN (5×10^{7} cm s^{-1}), and large conduction band offset. However, the fabrication of high-quality InN/GaN heterostructures is a challenging issue due to the difficulty in continuous growth of InN and GaN films because of large difference in the optimum growth temperature between them (InN ~500°C and GaN ~750°C). In addition, due to the low dissociation temperature of InN, it is very difficult to get high-quality InN/GaN heterostructure at the growth temperature of InN. In addition, the large lattice mismatch between InN and GaN (11%) results in a poor interface. Several groups [24–26] have studied the interfaces of the heterostructures like InN/GaN, GaN/ZnO, and GaN/AlN. InN/GaN MQWs with 1 and fractional monolayers of InN were proposed and experimentally demonstrated by Yoshikawa et al. [27]. Similarly, InN/GaN single-quantum well and double heterostructures were fabricated by the PAMBE [28]. In this section, InN/GaN heterostructures were grown using MBE system. InN thin films of thicknesses around 300 nm were epitaxially grown on 4 μm-GaN/Al_2O_3 (0 0 0 1) templates at different substrate temperatures. Thermal cleaning of the GaN templates was carried out at 700°C for 5 min in the presence of nitrogen plasma. Following that, a step growth method was employed to grow high-quality InN epilayers. The first step involved the growth of low-temperature InN nucleation layer at 400°C for 15 min, which resulted in the formation of thin buffer layer ~20 nm. Subsequently, the substrate temperature was increased to 450°C (sample A), 470°C (sample B), 500°C (sample C), and 530°C (sample D)

to grow active InN epilayers. The nitrogen flow rate and the forward RF power of the plasma source were set to 0.5 sccm and 350 W. The indium BEP was 1.53×10^{-7} mbar.

Figure 3(a) shows a 2θ-ω scan of InN films grown at different growth temperatures [29]. The peaks at $2\theta = 31.3$ and 65.5° are attributed to the (0002) and (0004) planes of the InN epilayers, whereas the peaks at $2\theta = 34.56$ and 72.81° are attributed to the (0002) and (0004) planes of the GaN templates. The peak at $2\theta = 41.69°$ corresponds to the (0006) plane of sapphire substrate. The InN films grown at low (450°C) and high (530°C) temperatures show a peak at around $2\theta = 33°$ indicating the presence of In metal. The presence of In metal could be due to the low migration of In at low temperature and more dissociation of InN at high temperature. The structural quality of the films was evaluated from the full width at half maximum (FWHM) of (0002) InN X-ray rocking curve (XRC). The rocking curves of the (0002) InN reflection are shown in **Figure 3(b)** [29]. Growth of InN epilayers at high temperature improved crystal quality, i.e., the FWHM of the (0002) InN XRC decreased from 532.8 to 450 arcsec corresponding to growth temperatures 450 and 500°C. The low migration velocities of In and N atoms at low growth temperature are the most probable reason for the relatively inferior crystal quality [30]. On the other hand, growth of InN at higher temperature (530°C) resulted in pronounced dissociation of InN, thus leading to high FWHM of 716.4 arcsec. The screw dislocation density of InN films, as calculated from the FWHM of the rocking curves, was found to be 2.27×10^8, 2.03×10^8, 1.62×10^8, and 4.12×10^8 cm^{-2} for samples A, B, C, and D, respectively. In addition, InN films show n-type conductivity with carrier concentrations in the order of 10^{18} to 10^{19} cm^{-3}. As growth temperature increases from 450 to 500°C, the carrier concentration decreases from 1.57×10^{19} to 3.10×10^{18} cm^{-3}. The high carrier concentration at low growth temperature may be due to relatively poor crystallinity. On the other hand, the carrier concentration increased to 1.10×10^{19} cm^{-3} at high growth temperature of 530°C, which may be associated with the large dissociation of InN.

The room temperature optical absorption spectra squared as a function of growth temperature is shown in **Figure 3(c)** [29]. The absorption spectrum exhibits characteristic interference fringes due to the underlying thicker GaN epilayer. The absorption edge of the InN films was estimated by extrapolating the linear part of the squared absorption down to the photon energy axis. The energy corresponding to this absorption edge is the amount of energy needed by an electron to make a vertical transition from the upper valence band to the Fermi surface in the conduction band. Therefore, this energy can be considered as the Fermi-level energy in the conduction band. A strong shift was observed in the absorption edge with a change in carrier concentration. This is usually referred as Burstein-Moss shift which is a commonly observed phenomenon in narrow-gap semiconductors owing to non-parabolic conduction band [31].

2.2. Nonpolar InN/GaN heterostructures

Growth of nonpolar a-plane InN/GaN heterostructures has been an important subject recently due to its potential improvement on the efficiency of III-nitride-based optoelectronic devices [32, 33]. However, growth of high-quality nonpolar InN/GaN heterostructures is challenging due to the low thermal decomposition temperature of InN film and high equilibrium vapor pressure of nitrogen. Despite the growth of high-quality nonpolar GaN films [23, 34, 35],

http://dx.doi.org/10.5772/intechopen.70219

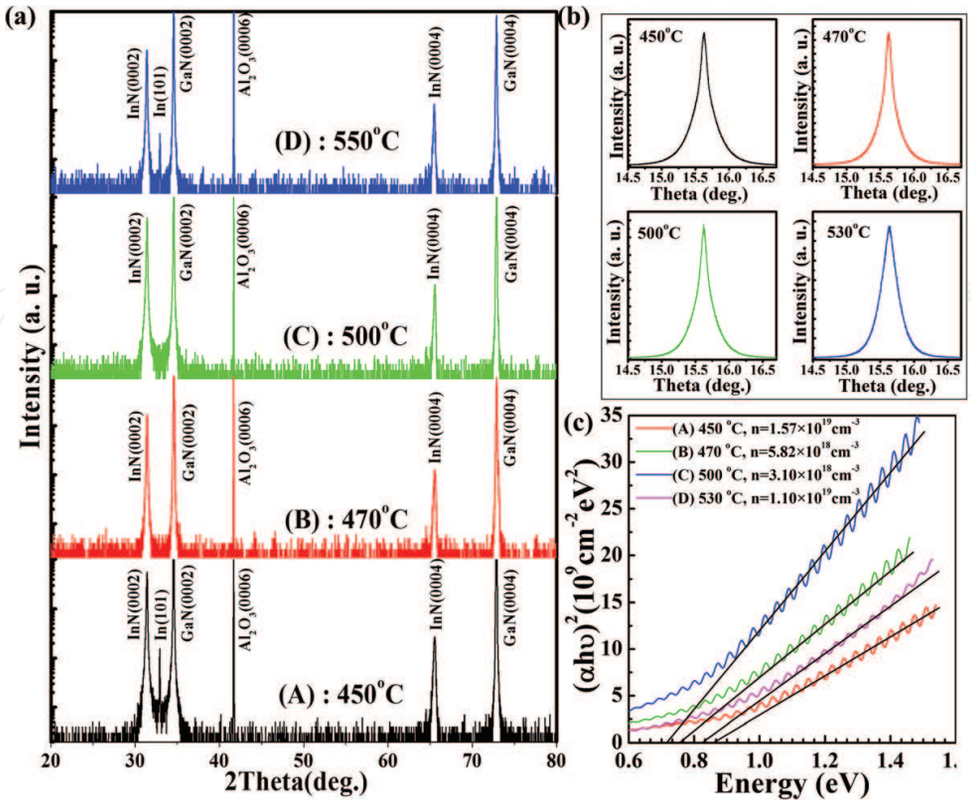

Figure 3. (a) 2θ-ω HRXRD scanning curve of InN films grown at different growth temperatures, (b) the XRC of the (0002) reflections of InN films grown at different growth temperatures, and (c) optical absorption spectra of InN films. Reprinted with permission from [29].

there are very few reports on the growth of nonpolar InN films [36, 37]. The earlier reports on the InN on r-sapphire substrates indicate the growth of cubic (001) [38, 39] and polar (0001) InN [40]. The nonpolar a-plane InN was demonstrated by using GaN buffer layer on r-plane sapphire [41, 42]. In this section, nonpolar (1 1 −2 0) a-InN/GaN heterostructures were grown on r-plane and m-plane sapphire substrates, respectively, using MBE system. Prior to the growth, thermal cleaning of the sapphire substrate was carried out at 850°C inside MBE chamber for 30 min under ultrahigh vacuum. RF power and flow rate were kept constant at 350 W and 0.5 sccm, respectively. (1 1 −2 0) a-GaN buffer layer was grown at 760°C temperature. The growth of InN epilayers was carried out using two-step growth processes: growth of low-temperature InN buffer layer (~20 nm) on GaN under layer at 400°C and growth of InN epilayers at different temperatures. The growth temperature of (1 1 −2 0) a-InN varied from 470 to 530°C.

Figure 4(a) show 2θ-ω scans of nonpolar (1 1 −2 0) a-plane InN/GaN heterostructures grown on r-plane sapphire substrate at different growth temperatures [42]. The peaks at 2θ = 57.7 and 51.61° are assigned to the a-plane GaN and a-plane InN reflections, respectively, along with that from the r-plane sapphire substrate. The sample grown at 530°C shows the peak at 32.9° which corresponds to In (101) reflections. **Figure 4(b)** shows the RHEED patterns in the azimuths [0001] for a-plane GaN and a-plane InN [43]. The Bragg spots appear with weak streaky lines in the RHEED patterns observed for a-plane GaN that confirms the reasonable smooth surface [44]. Spotty nature of a-plane InN RHEED pattern indicates the 3D growth of

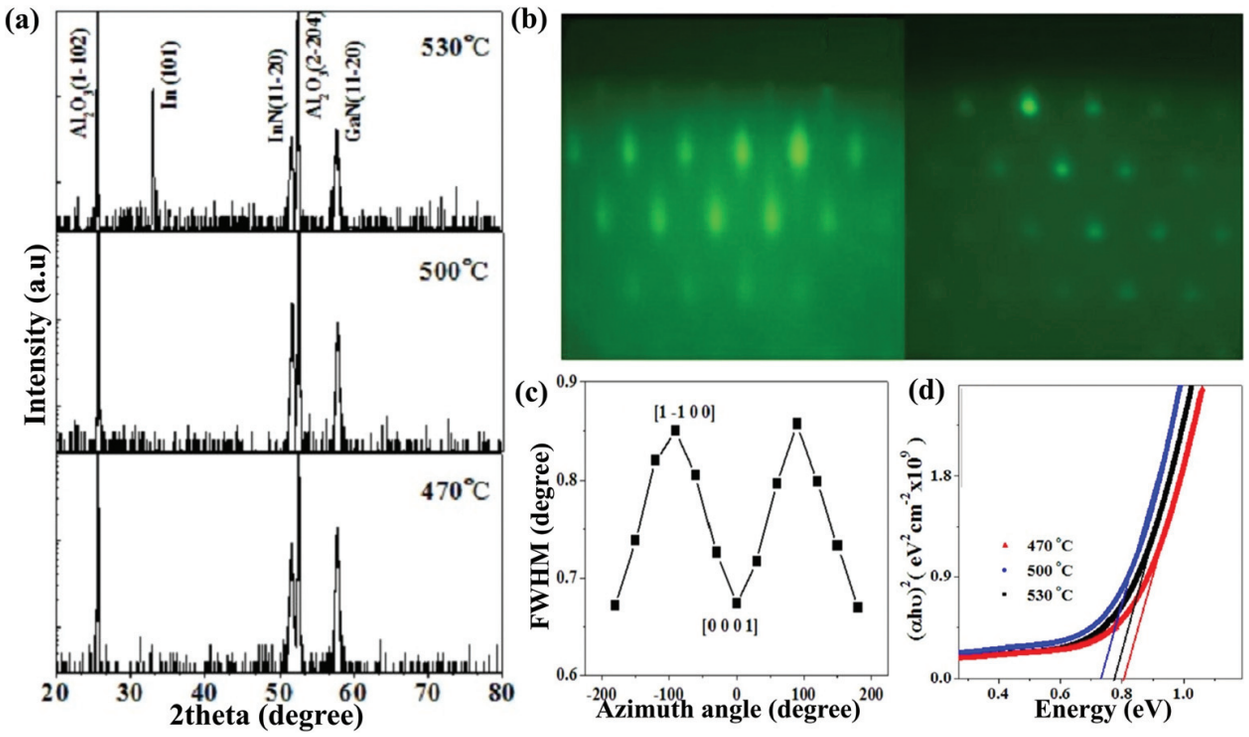

Figure 4. (a) 2θ-ω HRXRD scans of nonpolar a-plane InN film grown on GaN/r-Al_2O_3 substrate at different temperatures, (b) RHEED patterns of a-plane (11−20) GaN and a-plane (11−20) InN taken along (0 0 0 1) azimuth, (c) rocking curve FWHM of nonpolar a-plane InN grown at 500°C with different azimuth angles, and (d) optical absorption spectra of nonpolar a-plane InN. Reprinted with permission from [42, 43].

InN [43]. The X-ray rocking was carried out to see the structural quality of the samples. The FWHM of the rocking curve along with different azimuth angles has been plotted in **Figure 4(c)** for InN film grown at 500°C [42]. The variation of FWHM was found to be M-type with respect to the azimuth angles. The FWHM of the (1 1 −2 0) reflection was found to be strongly dependent on the azimuth angle with respect to the scattering plane. Azimuth angle was defined as zero when the incident beam is parallel to the [0001] direction. Darakchieva et al. reported similar kind of M-type behavior in a-plane InN epilayers grown on r-sapphire substrates with GaN buffer layer [45]. The FWHM of (1 1 −2 0) reflection along [0 0 0 1] and [1 −1 0 0] directions was determined, and the values are 0.67 and 0.85°, respectively.

Absorption spectroscopy was used to determine the bandgap of nonpolar a-plane InN films and is shown in **Figure 4(d)** [42]. The direct optical bandgap for InN can be investigated by fitting the absorption data. The bandgap of InN epilayers grown at 470, 500, and 530°C as obtained by fitting the absorption data is found to be 0.81, 0.74, and 0.78 eV, respectively. This shows that the bandgap of the samples grown at low temperatures is blue shifted with respect to the bulk, which could be due to the high background carrier concentration [46]. The carrier concentration of InN films was estimated by using Hall measurements, and the carrier concentrations was found to be in the order of 10^{18} to 10^{19} cm^{-3} with growth temperature. The film grown at 500°C showed the lowest carrier concentration, whereas the film grown at 470°C showed a higher carrier concentration due to the poor crystallinity. The carrier concentration in the film grown at 530°C was also found to be higher and could be as a result of high dissociation rate of InN at that temperature [47].

2.3. Polar InGan/GaN heterostructures

Indium gallium nitride (InGaN), a ternary compound of III-nitride semiconductors, has received considerable attention due to its potential applications in optoelectronic devices [48–51]. The choice of InGaN as an active layer in high-performance optoelectronic devices is due to the advantage one gets in tuning the energy bandgap from visible to near-ultraviolet region by changing the In composition. The most challenging issues in InGaN-based nitride semiconductors include the spatial fluctuation of indium composition and the generation of dislocations at the interface of InGaN-based heterostructures due to the limited solubility of indium atom into GaN because of the difference in the In-N and Ga-N bond length [52–54]. Because of dislocations the non-radiative recombination increases, leading to the rapid decrease in the performance of the InGaN-based devices [55, 56].

InGaN films of thicknesses around 200 nm were grown on 4 μm GaN/Al_2O_3 (0 0 0 1) templates using PAMBE. After the templates were chemically degreased, they were outgassed at 700°C for 5 min in the presence of nitrogen plasma. Followed by thermal cleaning, the InGaN films were grown in a single step. The indium composition was varied by changing the In/Ga flux ratio and substrate temperature, whereas the nitrogen plasma conditions were constant, flow rate ~0.5 SCCM and forward RF power of 350 W. **Figure 5(a)** shows a 2θ-ω scan of as-grown InGaN films [57]. Well-resolved peaks corresponding to InGaN (0002) reflection was observed along with the GaN and Al_2O_3 peaks in all the samples. The peaks at 2θ = 34.56 and 41.69° attribute to the (0002) planes of the GaN films and (0006) plane of the sapphire substrate, respectively. The indium concentration in the as-grown InGaN films was determined by linearly interpolating the peak position of (0002) plane from their end binaries, by assuming that Vegard's law is valid [58, 59]. The indium concentration obtained for InGaN films with different growth conditions is given in **Table 1**. For a constant In/Ga flux ratio (0.61), the decrease in growth temperature 600 to 550°C leads to the suppression of spinoidal decomposition. The transformation of multiple peaks to a single peak corresponding to InGaN (0002) planes is the evidence. The samples grown at high temperature, ~560°C, with high In/Ga flux ratio (0.99) showed similar single peaks. However, the presence of In (101) peak states that metallic In was also present. Further, it was also observed that at growth temperature ~560°C, the increase in In/Ga ratio from 0.61 to 0.99 not only led to increase in the In incorporation but also decreased the spinoidal decomposition. Therefore, we could obtain high-quality, metal-free, single composition InGaN epilayers with 23% indium (sample E) on GaN/c-Al_2O_3 when grown at 550°C with In/Ga ~0.61.

The X-ray rocking curve (XRC) was carried out to see the structural quality of the InGaN film. **Figure 5(b)** shows the XRC of the (0002) InGaN reflection of sample E [57], and the corresponding FWHM was found to be 390 arcsec, indicating the high quality of the as-grown InGaN film. This value is comparable to the values in literature [60, 61]. Though this value indicates the quality of bulk film, it doesn't tell us much about the interface dislocations. The influence of such interface defects on the barrier height, and the ideality factor will be discussed in further sections. **Figure 5(c)** shows the room temperature PL spectra of sample E [57]. As we can see from the PL spectra, the emission peak at 2.48 eV corresponds to the free excitonic transition between valence and conduction bands of InGaN film. Also, one can notice the presence of fringes around this peak, which are a result of Fabry-Perot interference, hence

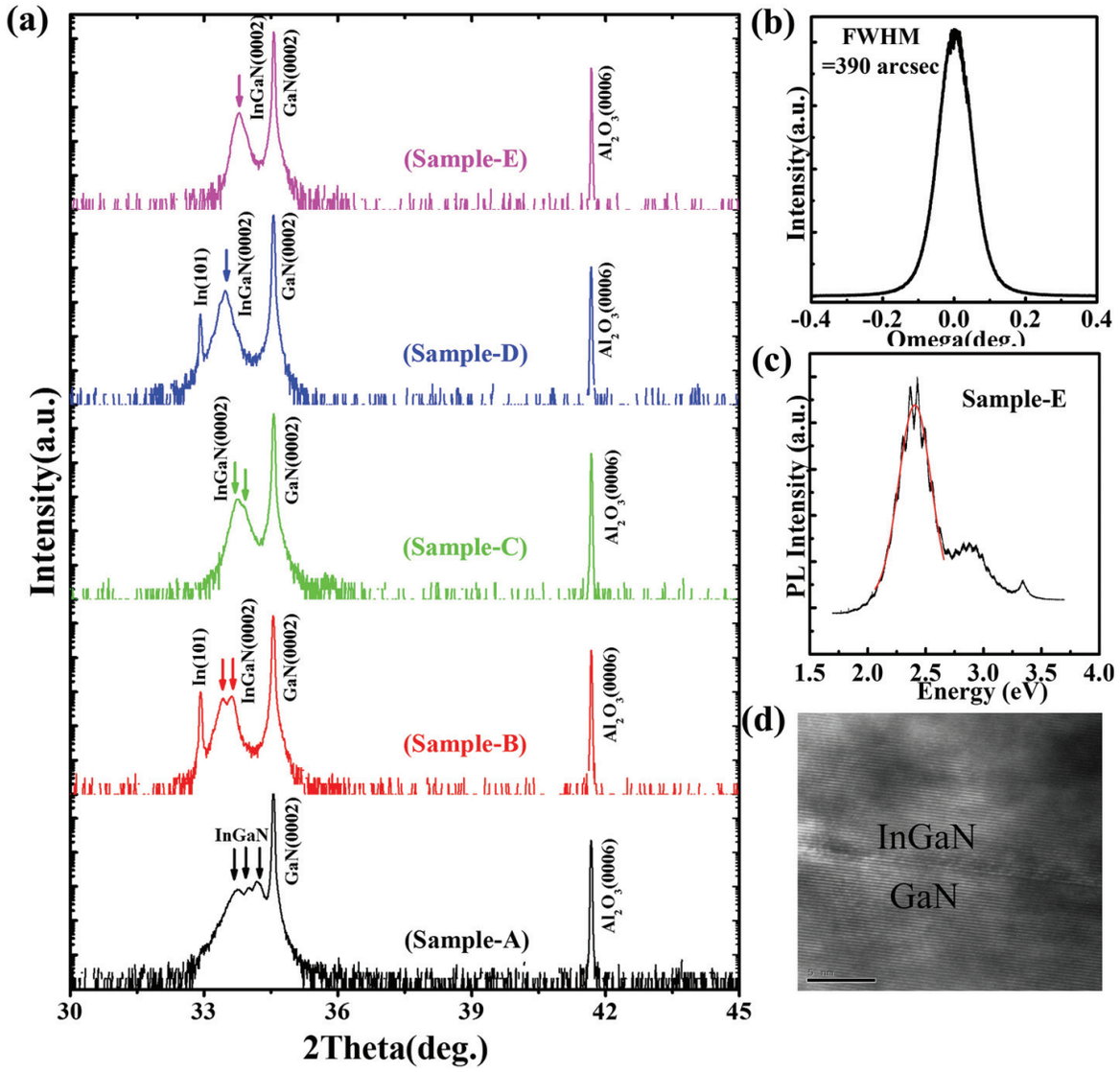

Figure 5. (a) 2θ-ω HRXRD scanning curve of InGaN films grown on GaN, (b) X-ray rocking curve of the (0002) plane of InGaN film (sample-E), (c) the room temperature photoluminescence spectra of InGaN film grown on GaN (sample E), and (d) HRTEM of InGaN/GaN interface. Reprinted with permission from [57].

Sample ID	In/Ga flux ratios	Growth temperature (°C)	In composition
Sample A	0.61	600	11, 16, 24%
Sample B	0.99	540	28, 35%
Sample C	0.61	560	20, 24%
Sample D	0.99	560	33% (In)
Sample E	0.61	550	23%

Table 1. Growth parameters used for the growth of InGaN films.

suggesting a smooth and abrupt interface. The film also exhibits a peak at 3.41 eV, which corresponds to underlying GaN layer. A second peak at 2.94 eV might correspond to the thin InGaN strain-relieving layer with ~6% of In [62, 63]. The indium composition of the InGaN

http://dx.doi.org/10.5772/intechopen.70219

layer was calculated using Vegard's law and was found to be 22% in sample E, which is in correlation with the value as estimated by HRXRD. **Figure 5(d)** is the high-resolution transmission electron microscopy (HRTEM), which showing an extremely sharp interface and the growth plane (0001) is perpendicular to the growth direction. High-quality interface as seen from the HRTEM image justifies the less defect densities and high crystallinity of the InGaN films.

2.4. Nonpolar InGaN/GaN heterostructures

InGaN alloys of various compositions are being optimized as materials for the fabrication of light-emitting diodes which are active in the entire visible spectrum extending up to ultraviolet wavelengths [32, 64]. Indium-rich InGaN alloys are now being considered potential candidates for longer wavelength emitters, thermionic emitters, multi-junction solar cells, etc. [65–67]. A concern with polar heterostructures is the intrinsic and strong polarization fields resident in the lattice. To overcome such polarization effect, substrates oriented in nonpolar directions, i.e., (1 0 −1 0) m-plane or (1 1 −2 0) a-plane, are used. Devices grown on these orientations are receiving a lot of focus due to this enhanced behavior. However, a slight compromise in terms of quality has to be made because of the large mismatch in lattice constants, thermal expansion coefficients, and elastic constants of InGaN and GaN. In addition, the large lattice constant mismatch between GaN and InN (~11%) results in a phase separation in InGaN alloys which has been theoretically predicted and experimentally observed [68]. This makes the growth of InGaN very challenging, especially for higher concentration of indium (>20%) [58]. Growth parameters such as growth temperature, growth rate, and flux ratio are seen to drastically affect the indium incorporation in InGaN films. During growth of the InGaN alloys, the evaporation of indium species from the surface will be suppressed at lower temperatures and leads to higher growth rates as the indium species become trapped by the growing layer [69, 70]. As the indium content in the InGaN alloy increases, the material quality degrades due to phase separation, inhomogeneity of solid solution, and indium metal droplets. Few reports are available in the literature for the study of the nonpolar InGaN-based multiple quantum well (MQW) structures and other devices. Song et al. studied the effect of periodicity of a-plane InGaN/GaN multiple quantum wells on the output power of the LEDs grown by MOCVD [71].

In this section, $In_xGa_{1-x}N$ films of thicknesses around 125 nm were grown on 125 nm a-GaN (11−20)/r-Al_2O_3 (1−102) by PAMBE system. A two-step growth process was employed to grow a-GaN film, which constituted the growth of a 20 nm thin low-temperature GaN buffer layer at 500°C and a ~125nm GaN epilayer at 760°C. The nitrogen plasma RF power and N_2 flow rate were kept constant at 350 W and 1 sccm, respectively, throughout the growth duration. The gallium beam equivalent pressure (BEP) was kept at 5.6×10^{-7} mbar, corresponding to the growth in the slightly nitrogen-rich region. $In_xGa_{1-x}N$ films were grown on top of the a-GaN layer at the growth conditions as tabulated in **Table 2**. Three $In_xGa_{1-x}N$ films (samples A, B, and C) with different indium compositions were grown by varying the In/Ga flux ratios and growth temperatures. During the $In_xGa_{1-x}N$ growth, the nitrogen flow rate and RF power of the plasma source were kept at 0.5 sccm and 350 W, respectively.

Figure 6(a) shows the 2θ-ω HRXRD scan of the grown films, which confirmed the growth of nonpolar a-InGaN epilayer oriented in the (1 1 −2 0) direction and a-GaN epilayer oriented in

Sample ID	Gallium BEP (mbar)	Indium BEP (mbar)	Growth temp. (°C)
(A)	1.23×10^{-7}	1.17×10^{-7}	550
(B)	1.23×10^{-7}	8.87×10^{-8}	550
(C)	1.23×10^{-7}	8.87×10^{-8}	540

Table 2. Growth conditions for a-$In_xGa_{1-x}N$/a-GaN/r-sapphire substrate.

the (1 1 −2 0) direction on (1 −1 0 2) r-plane sapphire. The peak at 2θ = 56.64° for sample A, 2θ = 56.59° for sample B, and 2θ = 56.36° for sample C was assigned to (1 1 −2 0) $In_xGa_{1-x}N$ which corresponds to the different composition of indium in the grown films. The calculated compositions of the samples were $In_{0.17}Ga_{0.83}N$ (sample A), $In_{0.19}Ga_{0.81}N$ (sample B), and $In_{0.22}Ga_{0.78}N$ (sample C). We observe that by decreasing the indium flux during the growth from 1.17×10^{-7} to 8.87×10^{-8}, we could incorporate more indium into the $In_xGa_{1-x}N$ alloy. Higher indium incorporation was also observed when the substrate temperature was decreased from 550C to 540°C keeping the indium flux constant. Growth parameters play a very critical role in controlling the composition of the $In_xGa_{1-x}N$ films. For the given set of growth parameters, we have not observed any phase separation or indium segregation in the grown $In_xGa_{1-x}N$ films.

X-ray rocking curve (ω) analysis was carried out to determine the crystal quality of the as-grown structures. Rocking curves along different azimuth angles have been recorded, and RC FWHM versus azimuth angle has been plotted for all the samples as shown in **Figure 6(b)**. The RC FWHM of the reflection along the normal varied with the azimuth angle and showed an M-type behavior [72]. The measured FWHM value of (1 1 −2 0) reflection of $In_{0.22}Ga_{0.78}N$ along [0001] direction defined as azimuth angle 0°and along [1−100] direction defined as azimuth angle 90° was found to be 0.532 and 0.703°, respectively. The RC FWHM values of (1 1 −2 0) GaN reflections were found to be 0.47 and 0.52° along azimuth angle 0° corresponding to reflection along [0001] direction and 90° corresponding to reflection along [1−100] direction, respectively. The reason behind the broadening of InGaN rocking curves could be attributed to the presence of defects such as partial dislocations and stacking faults, thus suggesting that the crystalline quality of nonpolar InGaN films is reduced with the increase in indium incorporation [73]. Cross-sectional plan view of TEM image obtained in bright field is shown in **Figure 6(c)**, which shows a clear interface of the a-InGaN/a-GaN/r-sapphire structure. The thickness of the each layer grown is confirmed from the image to be around 125 nm each. Basal stacking faults (BSF) are visible as thin lines, and they arise from the low-temperature nucleation layer. Due to the anisotropic nature of the growing surface, the nonpolar GaN typically has a high density of BSFs. The room temperature PL spectrum of $In_xGa_{1-x}N$ films is shown in **Figure 6(d)**. The position of the near-band-edge emission (NBE) of the $In_xGa_{1-x}N$ as observed for the three samples were 2.67, 2.59, and 2.56 eV for samples A, B, and C, respectively. Using Vegard's law, the values of indium fraction were found to be 0.20, 0.22, and 0.23 for samples A, B, and C, respectively.

Reciprocal space maps (RSMs) were recorded to look into the microstructure and strain present in the films. The reciprocal lattice points (RLPs) will be elongated along the Q_x axis if the broadening is caused by the limited mosaic block dimensions [74]. The RLPs will be tilted

http://dx.doi.org/10.5772/intechopen.70219

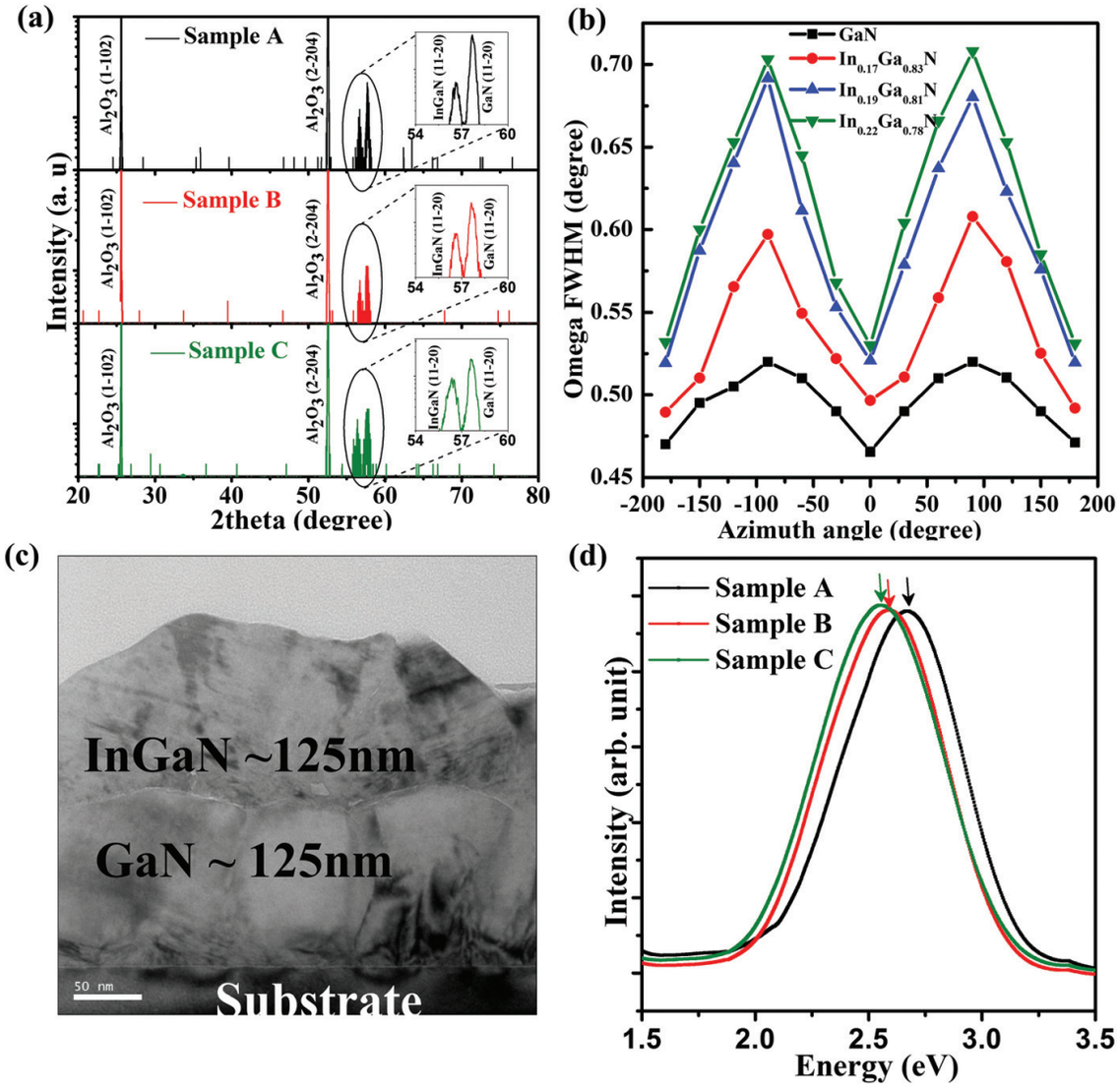

Figure 6. (a) HRXRD 2θ-ω scan of nonpolar (11−20) a-InGaN epilayer grown on (11−20) a-GaN/(1−102) r-plane sapphire, (b) FWHM of the rocking curve along with variation in azimuth angles for InGaN and GaN layer, (c) bright-field plan-view cross-sectional image of a-InGaN/a-GaN/r-sapphire substrate, and (d) room temperature PL spectrum of $In_xGa_{1-x}N$ films.

in the reciprocal space if additional mosaic tilt exists in the sample. From **Figure 7(a)–(c)**, the RLPs along the symmetric (1 1 −2 0) reflection of all samples are all broadened in the Q_x direction with negligible inclination, indicating that the dominant broadening mechanism for it is the limited mosaic block size. Asymmetric reflection are expected to be elongated parallel to the lateral scattering vector if the material experiences broadening due to short-sized mosaic blocks and could be also inclined if an additional mosaicity tilting exists in the material [75]. To understand the strain in the film with respect to the substrate, asymmetric RSM along (1 0 −1 0) a-GaN scans were obtained and are shown in **Figure 7(d)–(f)**. Shift of the center of each peak along the Q_z axis in an asymmetric scan gives a direct evidence of the strain present between the layers. Splitting of the GaN peak for all compositions implies a formation of a thin layer of high gallium composition $In_xGa_{1-x}N$ layer which is highly strained with respect to the GaN

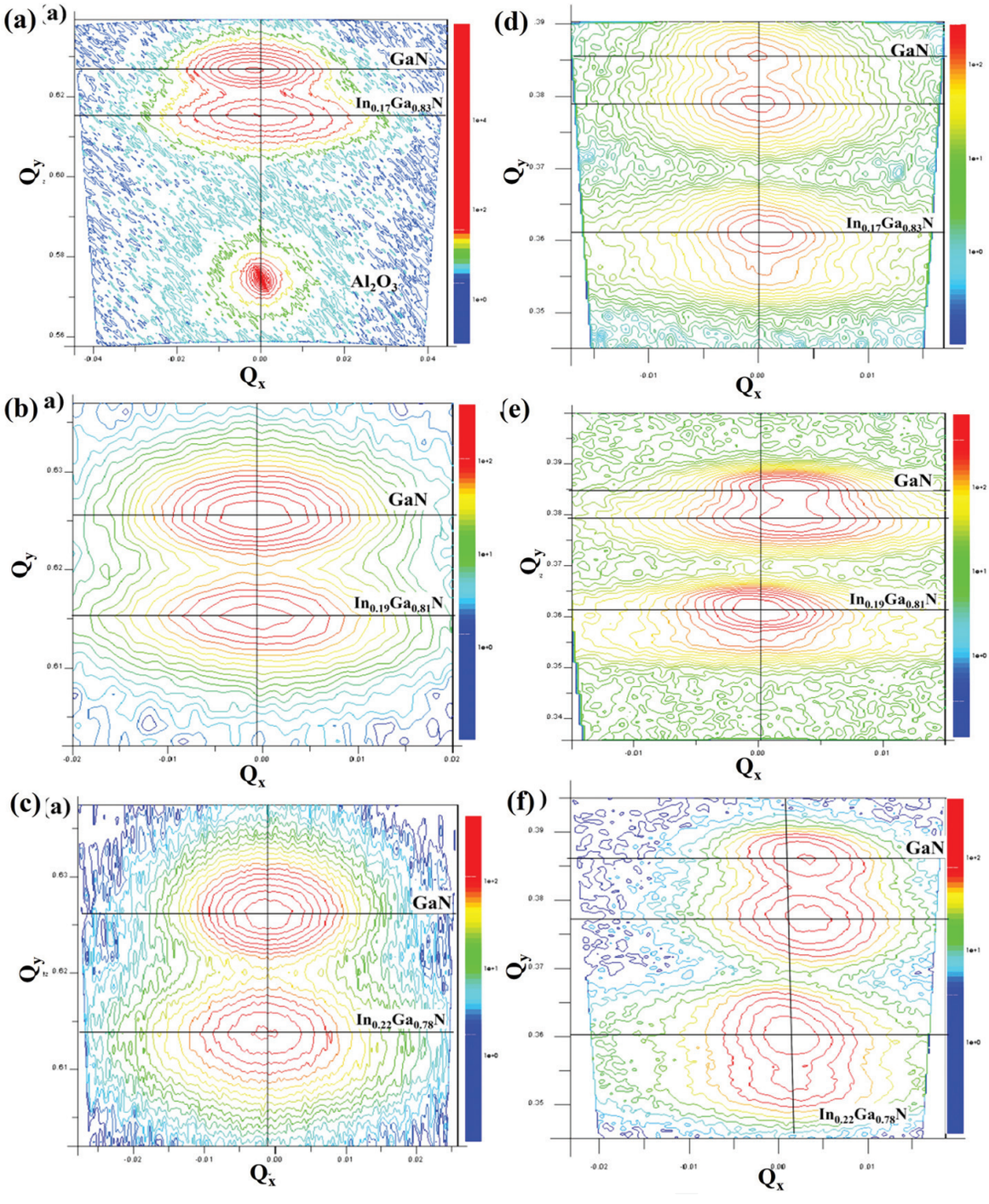

Figure 7. (a)–(c) RSM of symmetric (1 1 −2 0) of $In_xGa_{1-x}N$/GaN/r-sapphire and (d)–(f) RSM of asymmetric (1 0 −1 0) $In_xGa_{1-x}N$/GaN layers.

layer. Hence, from the asymmetric RSM scans, it is understood that after a thin layer of $In_xGa_{1-x}N$ acting as a buffer layer, the $In_xGa_{1-x}N$ film with In concentration of 17, 19 and 22% was formed in samples A, B, and C, respectively. As the In concentration is increased, the InGaN film is showing signs of relaxation which indirectly means increase in the dislocation density, reducing the crystallinity of the layer which is consistent with the observation of the variation of FWHM in rocking curve measurements.

2.5. InGaN/Si heterostructures

n-n heterojunctions have found use in different applications such as photodetectors, light-emitting diodes, solar cells, injection lasers, etc. [76–80]. So far the most extensively studied material systems are ZnO/Si, $In_xGa_{1-x}As$, $In_xGa_{1-x}Sb$, Ge-Si, etc. [81, 82]. Very few groups have reported studies on isotype heterojunctions of $In_xGa_{1-x}N$ system [83, 84]. The large lattice mismatch of InGaN with silicon substrates has hindered the realization of silicon-based commercial devices and is limited to sapphire which happens to be an insulator. Therefore, obtaining smooth and abrupt heterojunctions with minimum density of interface defects by overcoming the lattice mismatch issue has been a concern of great interest for many researchers across the globe. Several attempts have been made to demonstrate low power consuming or self-powered photodetectors [85, 86]. There are a few reports on the UV photodetection using InGaN as an active layer [87]. In this work, we report the development of a UV photodetector which is operated at zero bias. The device comprises of a simple n-InGaN/n-Si heterojunction. The role of interface defects originating due to the large lattice mismatch, such as traps, in modulating the built-in electric field driven photoresponse has been discussed. The n-Si (111) substrates of 1×1 cm^2 in size were cleaned chemically by trichloroethylene, acetone, and methanol and were dipped in 5% HF for 60 s to remove the native oxide prior to loading in the growth chamber. Thermal cleaning of Si (111) was carried out at 900°C for the removal of native oxide layer. The substrate temperature was further reduced to 550°C, and growth was carried out for 2 h without any intermediate steps. The indium (In) beam equivalent pressure (BEP) and gallium (Ga) BEP, nitrogen flow, and plasma power were kept at 8.52×10^{-8} mbar, 1.2×10^{-7} mbar, 1 sccm, and 350 W, respectively. Various experimental techniques were employed to study the as-grown samples as mentioned in upcoming sections. Circular aluminum contacts with diameters of 600 μm were then deposited by thermal evaporation on the InGaN films and Si (111) substrate with the help of a physical mask to study the current-voltage and photoresponse studies.

Figure 8(a) shows the 2θ-ω HRXRD scan of InGaN epilayers on Si (111) substrates [88]. The peaks at 2θ = 28.45 and 58.86° attribute to Si (111) and Si (222) reflections, respectively. The peaks at 2θ = 34.05 and 71.89° correspond to (0002) and (0004) reflections of InGaN. Also, no secondary phases or residual indium or InN phases were found, confirming that the films are single crystalline. The In composition was determined to be 15% from the linear interpolation of the 2θ peak positions of (0002) GaN (34.59°) and (0002) InN (31.22°). In **Figure 8(b)** the rocking curve FWHM value (degree) of asymmetric reflection (2.16) is higher than that of the symmetric reflection (2.05), which attributes to the presence of large edge threading dislocations (TDs) [73].

The room temperature PL spectra of the $In_xGa_{1-x}N$ films are shown in **Figure 8(c)**. Near-band-edge emission peaks are observed at 502.12 nm corresponding to the bandgap of 2.46 eV. Due to stoke shift of the PL spectra and discrepancies in the exact value of InN, bandgap [89] further adds ambiguity to the exact In content determination from PL spectra. A small hump is observed around 425 nm which might be due to the initial layers with a large number of dislocations arising due to the large lattice mismatch of Si and InGaN films [90]. One can also correlate the presence of a large number of defects from the FWHM values of both symmetric

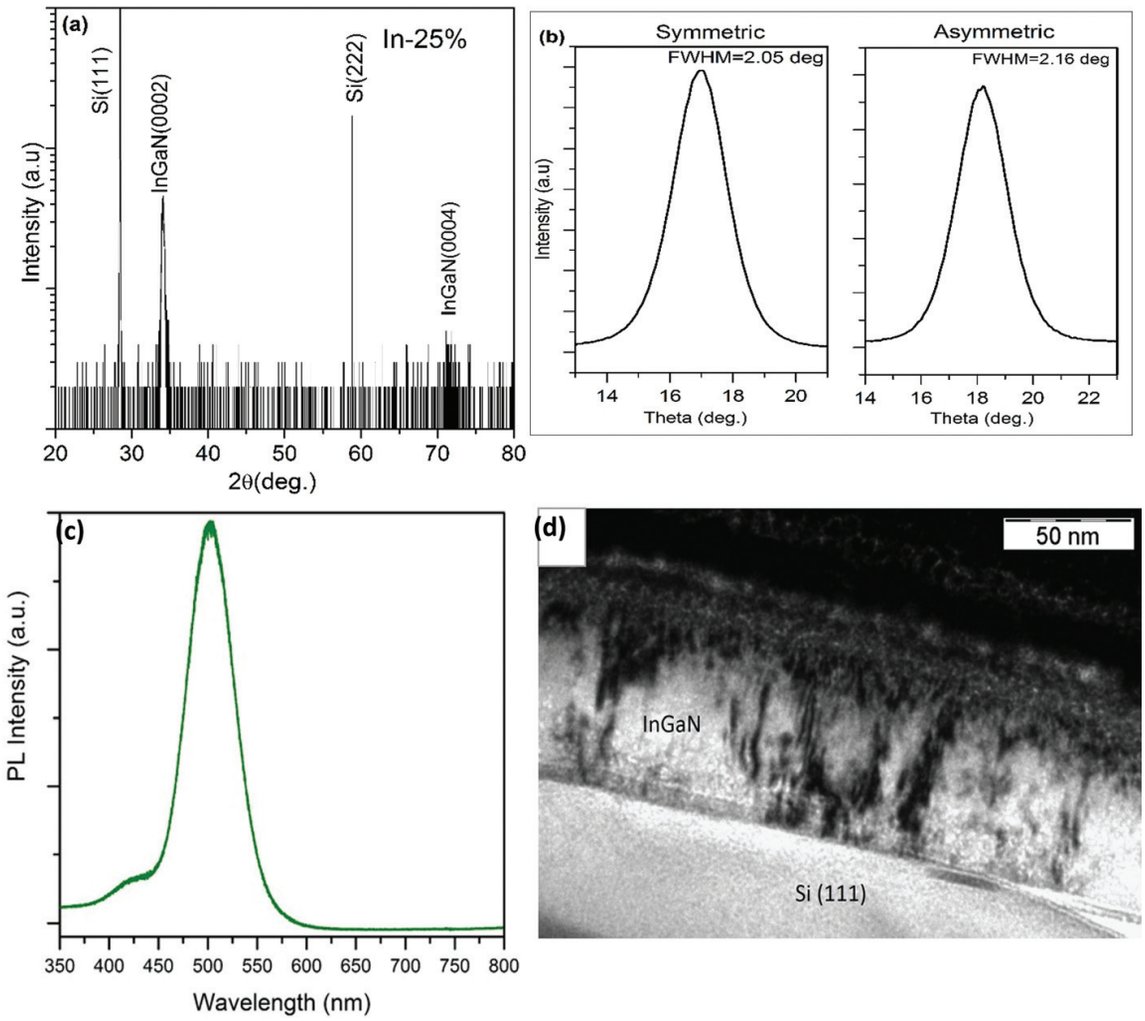

Figure 8. (a) HRXRD 2θ-ω scan of InGaN on bare Si (111), (b) X-ray rocking curve of (0002) and (10−11) reflections, (c) photoluminescence spectra of InGaN/Si, and (d) cross-sectional TEM of InGaN/Si heterostructure. Reprinted with permission from [88].

and asymmetric XRCs. The contrast at the interface in the TEM image in **Figure 8(d)** clearly indicates the presence of initial low-contrast Ga-rich layers which possibly attribute to the ~425 nm peak in PL spectra. The thickness was estimated to be ~100 nm from the TEM image. The other dark regions are formed as a result from the Ga ion beam damage during sample thinning.

3. Transport properties of III-nitride heterostructure-based Schottky junctions

3.1. Polar and nonpolar InN/GaN heterostructures.

The semiconductor heterostructure exhibits the Schottky barrier at the interface due to the formation of conduction band offset because of their different bandgap values. The concepts on the band offset are directly transferable to the Schottky barrier height problems. Hence, it is

http://dx.doi.org/10.5772/intechopen.70219

vital to study the transport properties of the semiconductor heterostructure-based Schottky junctions. The InN/GaN heterostructure has a large conduction band offset, thus ensuring effective blockage of the conduction current over the barriers [91, 92], which help for the development of electronic devices operating in THz frequency range [91]. Hence, studying the transport properties across the InN/GaN interface is very important from device view point. Chen et al. [93] studied temperature-dependent current-voltage characteristics of InN/GaN-based Schottky junctions in the range of 300–400K and found that the barrier height (~1.25 eV) and the ideality factor (~1.25) are nearly temperature independent. Similarly, Wang et al. [94] employed capacitance-voltage measurement technique to determine the Schottky barrier height to be 0.94 eV at room temperature. This section presents the study of the temperature-dependent electrical transport properties of InN/GaN heterostructures and observed the temperature-dependent barrier height and the ideality factor. **Figure 9(a)** shows the room temperature *J-V*(current density-voltage) characteristics for the junction. The junction between InN and GaN exhibits a rectifying behavior which suggests an existence of Schottky barrier height at the junction [95, 96].

To investigate further, we have studied the temperature-dependent *J-V (J-V-T)* characteristics ranging from 200 to 500 K and is given in **Figure 9(b)** [95]. In the present case, the GaN film is highly doped with silicon ($N_D \sim 1.4 \times 10^{18}$ cm^{-3}) resulting in a lower barrier height at the InN/GaN interface, which is due to the tunneling of charge carriers through the interface. This kind of behavior reveals that the current transport is primarily dominated by thermionic field emission (TFE) mechanism, where the carriers tunnel from GaN to InN. According to the transport theory, TFE dominates only when $E_{00}/kT \approx 1$, where E_{00} is the characteristic tunneling energy which determines the nature of conduction mechanism. When $E_{00}/kT \approx 1$, the Boltzmann distribution tail of thermionic emission drops off by a factor of $exp(-1)$, which is much faster than the decrease rate of the tunneling probability. On the other hand, thermionic emission (TE) is predominant when $E_{00}/kT << 1$ because the tunneling probability drops off faster than TE [97]. In the present case, the value of the barrier height and the ideality factor (η)

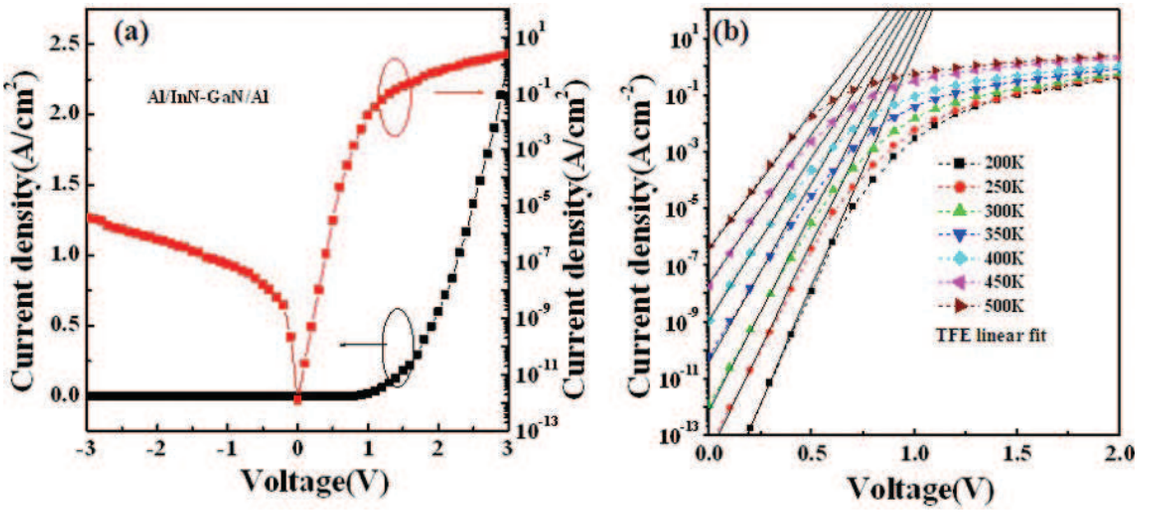

Figure 9. (a) The room temperature *J–V* characteristics of InN/GaN Schottky junction and (b) the forward *J–V* characteristics with TFE fitting as a function of measurement temperature. Reprinted with permission from [95, 96].

were calculated by fitting a line in the linear region of the forward J-V curves using the TFE equation and are shown in **Figure 9(b)**. From the abovementioned analysis, the barrier height and the ideality factor are found to be temperature dependent. Thus, our results indicate the presence of inhomogeneity at the interface due to the presence of various types of defects, which is why we observe the temperature-dependent behavior of barrier height [98, 99]. From the fitting the value of E_{00}/kT is observed to be nearly one, suggesting that the TFE conduction mechanism would be considered to be a more realistic model for the analysis of the electronic transport in polar InN/GaN heterostructure.

An optoelectronic device based on nonpolar III-nitride heterostructure has been an important subject due to its potential improvement on the efficiency. However, the transport behavior of nonpolar a-plane InN/GaN heterostructure interfaces is limited. In this section, we will discuss our results on the transport properties of nonpolar a-plane InN/GaN heterostructure. The inset of **Figure 10(a)** shows the schematic diagram of InN/GaN heterostructure Schottky junction. **Figure 10(a)** shows the room temperature *I-V* characteristic of nonpolar a-plane InN/GaN heterostructure Schottky junction [43]. The rectifying behavior of the *I-V* curve indicates the existence of Schottky barrier at the nonpolar InN/GaN interface. The forward bias *J-V*

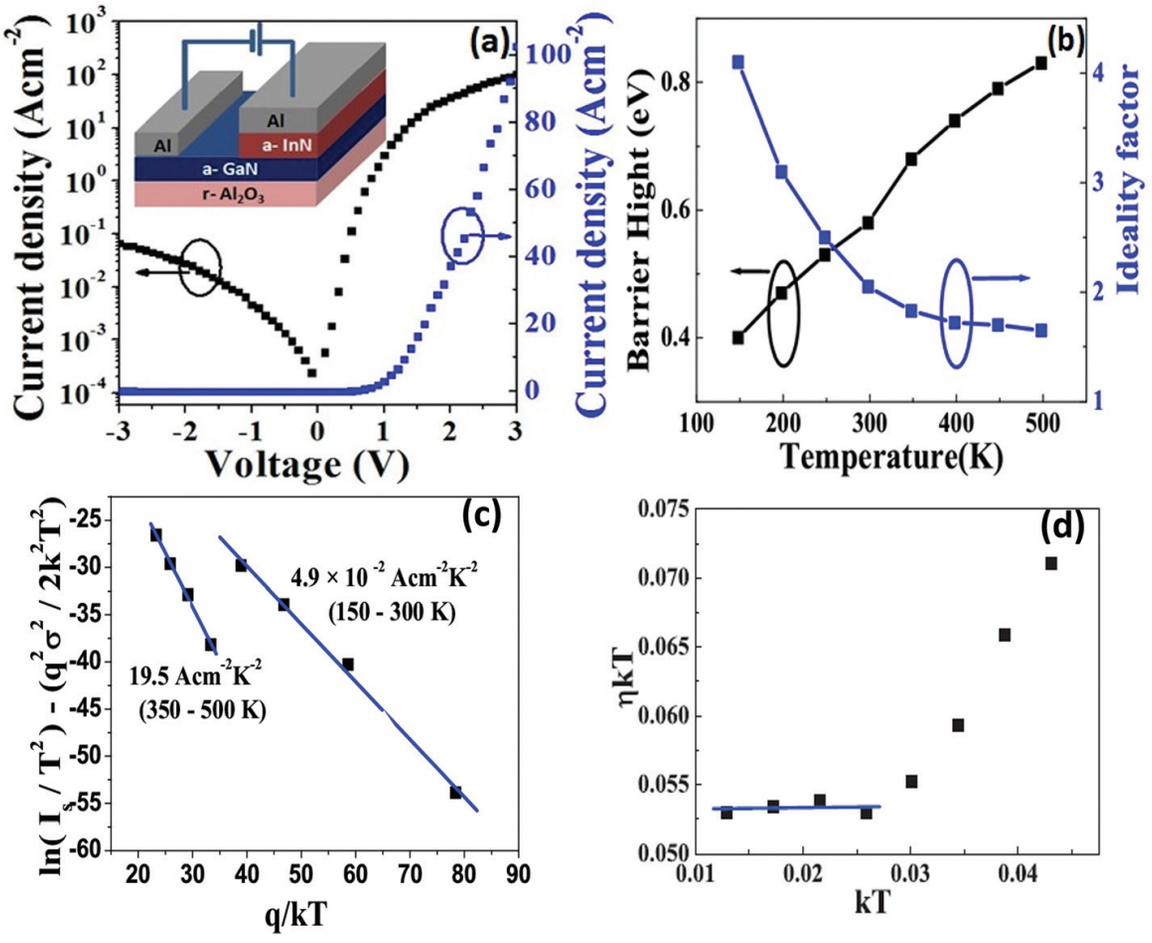

Figure 10. (a) Room temperature *I–V* characteristics of the nonpolar *a*-plane InN/GaN heterostructures, (b) temperature-dependent barrier height and the ideality factor, (c) modified Richardson plot of $ln(Is/T^2)$-$q^2\sigma^2/2k^2T^2$ versus q/kT, and (d) plot of ηkT as a function of kT. Reprinted with permission from [43, 96].

characteristics of the InN/GaN heterostructure were measured at different temperatures. The values of the barrier height and ideality factor were estimated by fitting the linear region of the forward *J-V* curves using thermionic emission model. It was found that the ideality factor and the barrier height values range from 1.65 and 0.83 eV (500 K) to 4.1 and 0.4 eV (150 K), respectively, as shown in **Figure 10(b)**. The variation of barrier height and the ideality factor with the measurement temperature indicates the presence of inhomogeneous nature of non-polar InN/GaN interface.

The inhomogeneous nature of barrier height at the InN/GaN interface could arise due to the presence of various types of defects at the interface [98, 99]. The inhomogeneous nature at the interface was explained by using Richardson plot of saturation current. In the Richardson plot, we could identify two separate temperature ranges, i.e., 150–300 and 350–500 K from the slopes, and the values of Richardson's constants (A^*) were found to be much lower than the theoretical value of 24 $Acm^{-2}K^{-2}$ for n-GaN. This type of barrier height inhomogeneity at the InN/GaN interface can be explained by considering the Gaussian distribution of barrier heights at the interface [100, 101] and can be written as

$$P(\varphi_b) = \frac{1}{\sigma_s\sqrt{2\pi}}\exp\left[-\frac{\left(\varphi_b - \overline{\varphi_b}\right)^2}{2{\sigma_s}^2}\right] \tag{2}$$

where $1/\sigma_s\sqrt{2\pi}$ is the normalization constant and $\overline{\varphi_b}$ and σ_s are the mean and standard deviation of barrier height, respectively. Considering Gaussian distribution of barrier height, the effective barrier height, φ_b, given by the expression

$$\varphi_b = \overline{\varphi_{b0}} - \frac{q{\sigma_s}^2}{2kT} \tag{3}$$

Here, $\overline{\varphi_{b0}}$ is the zero bias mean barrier height. Considering the barrier height inhomogeneities, the conventional Richardson plot is modified as follows:

$$\ln\left(\frac{I_s}{T^2}\right) - \left(\frac{q^2{\sigma_s}^2}{2k^2T^2}\right) = \ln(AA^*) - \frac{q\overline{\varphi_{b0}}}{kT} \tag{4}$$

Figure 10(c) shows the modified Richardson plot. In the first region (300–500 K), the values of $\overline{\varphi_b}$ and A^* were found to be 1.15 eV and 19.5 $A/cm^2\,K^2$, respectively. The calculated Richardson constant value in the temperature range of 350–500 K is very close to the theoretical value of 24 $A/cm^2\,K^2$ for n-type GaN. This indicates that at higher temperatures (350–500 K) the current transport is dominated by thermionic emission mechanism. The values of $\overline{\varphi_b}$ and A^* for polar c-plane InN/GaN heterojunction were found to be 1.6 eV and 25.8 $A/cm^2\,K^2$, respectively [102]. The reduced barrier height in nonpolar a-plane InN/GaN heterojunction when compared to the polar c-plane InN/GaN can be attributed to the absence of polarization field at the interface. The value of A^* is largely deviated in the temperature range of 150–300 K indicating the reduced dominance of thermionic emission. **Figure 10(d)** shows $E_0 = \eta kT$ versus kT plot for the nonpolar a-InN/GaN Schottky diode. The value, E_0, seems to be independent of temperature at

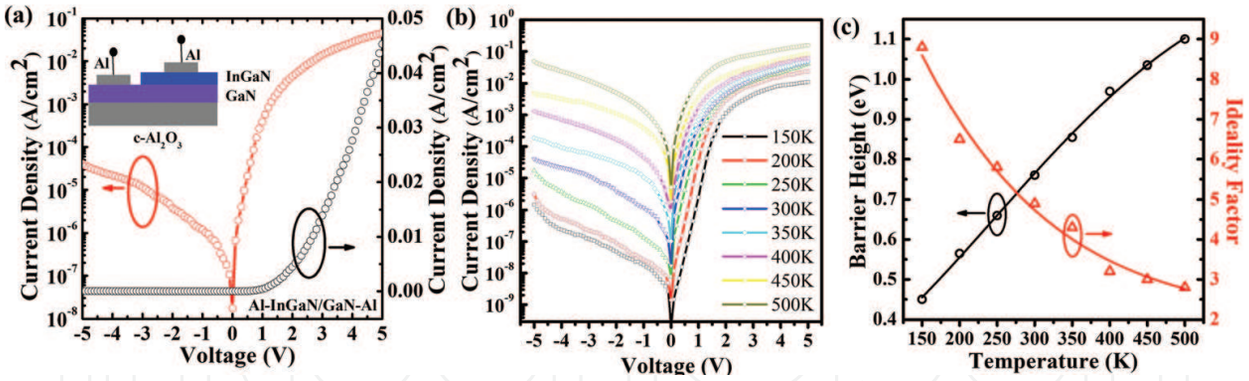

Figure 11. (a) Room temperature *J-V* characteristics of the InGaN/GaN heterostructure, (b) temperature-dependent *J-V* characteristics of the InGaN/GaN heterostructure, and (c) variation of the barrier height and the ideality factor with measurement temperature. Reprinted with permission from [104].

low temperatures, thus indicating the dominance of field emission in the range of 150–500 K [103]. It can be understood that the carriers lack the required energy to surmount the barrier at the low temperature and thus tunnel through the defect states at the interface.

3.2. Polar InGaN/GaN heterostructures

In this section, we have grown InGaN/GaN heterostructures using plasma-assisted molecular beam epitaxy and studied the temperature-dependent electrical transport characteristics. **Figure 11(a)** shows the room temperature *J-V* characteristics of the InGaN/GaN heterostructure in both linear and semilog scale [104]. The schematic diagram of the device structure has been shown in the inset of **Figure 11(a)**. The rectifying nature of *J-V* characteristic of InGaN/GaN heterostructure suggested the presence of a Schottky barrier at the interface. The temperature-dependent *J-V* characteristic of the heterostructure is shown in **Figure 11(b)**. It is observed that, as the measurement temperature increases, the forward bias current increases, which indicate that the current transport across the Schottky junction is governed by the thermionic emission mechanism. Then, the values of barrier height and ideality factor were calculated by using thermionic emission model. **Figure 11(c)** shows the variation of barrier height and ideality factor with measurement temperature [104]. It is observed that there is a temperature-dependent variation of both barrier height and ideality factor. The temperature dependence of φ_b indicates that the barrier height is inhomogeneous in nature, which may be due to various types of defects present at the InGaN/GaN interface. Moreover, the observed ideality factor greater than unity indicates a nonideal nature of the heterojunction, which is attributed to the presence of interface defect states.

4. InGaN/Si heterostructure-based UV and IR photodetectors

Room temperature *I-V* measurements were performed on InGaN/Si (111) heterojunctions with Si biased positively and were shown in **Figure 3(a)**. From **Figure 3(a)**, it is observed that the device is showing rectifying characteristics, both in the dark (room temperature as well as low

temperature) and under ultraviolet radiation, which are consistent with the n-n isotype heterojunctions of other materials as reported by others [81, 82, 105]. *I-V* characteristics were obtained on Al/InGaN/Si(111)/Al, Al/InGaN/Al, and Al/Si (111)/Al. The behavior of Al/InGaN/Al and Al/Si (111)/Al was ohmic and that of the Al/InGaN/Si (111)/Al junction was rectifying, thus confirming that the rectifying characteristic is primarily arising from the n-InGaN/n-Si isotype heterojunction. Although it seems to be like a leaky rectifying behavior, subsequent low-temperature current-voltage measurements were carried out to further confirm the rectifying behavior. Hall measurements were carried out, and negligible changes were observed at low temperatures in conductivity, mobility, carrier concentration, etc. The room temperature conductivity, mobility, and bulk carrier concentration of the InGaN layer were found to be ~201 $(\Omega\ \text{cm})^{-1}$, ~17 cm^2/Vs, and ~8×10^{19} cm^{-3}. The high background electron concentration (~10^{19}–10^{21}) is a well-observed characteristic of the undoped InGaN and InN due to the nitrogen vacancies in the bulk and along the edge dislocations at the interface and In vacancy/N antisite complexes [106] which explains the source of doping in our case. A detailed study on the current-transport mechanisms can be found elsewhere [88].

Although the device is not perfectly rectifying at room temperature, the interesting characteristics observed were in the region of zero bias. An abrupt increase in photocurrent in the presence of UV radiation was observed at zero bias than either reverse or positive biases and is shown in the inset of **Figure 12(a)**. Ager et al. [83] have shown the operation of similar devices in photovoltaic mode. However, the InGaN films grown on their samples were much thicker compared to the present work and also used several buffer layers. The photocurrent response and stability were studied from the on-off cycles of a UV lamp at zero bias and different voltages and are shown in **Figure 12(b)**. The order of increase in the photocurrent magnitude is higher in case of zero bias (>1.5) than that of the positive and reverse bias. **Figure 12(c)** and **(d)** shows the growth and decay responses which can be described as [107]

$$I(t) = I_{dark} + A\left[1 - \exp\left\{\frac{-(t - t_0)}{\tau_g}\right\}\right] \tag{5}$$

$$I(t) = I_{dark} + A\left[\exp\left\{\frac{-(t - t_0)}{\tau_g}\right\}\right] \tag{6}$$

for growth and decay, respectively, where I_{dark} is dark current; A is scaling constant; t_0 is the time when UV lamp was switched on or off for growth or decay, respectively; and τ_g and τ_d are growth and decay times. The response times obtained from the above equations are 20 and 33 ms for growth and decay. The responsivity (R_λ) of this photodetector is calculated from, $R_\lambda = I_\lambda / P_\lambda S$, where I_λ is photocurrent, P_λ is the incident power of UV lamp of wavelength, and S is the area of illuminated junction which is 0.09 cm^2. The external quantum efficiency (EQE) is given as $EQE = hcR_\lambda / e\lambda$, [108]. The values obtained for spectral responsivity and external quantum efficiency are 0.0942 A/W and 32.4%, respectively, which are better than the values reported in the literature [85] for such devices. The responsivities and external quantum efficiencies in case of different biases were found to be better than zero bias (**Table 3**). From **Figure 12(b)**, it can be seen that the photocurrents obtained at different biases do not overlap, i.e., the photocurrent

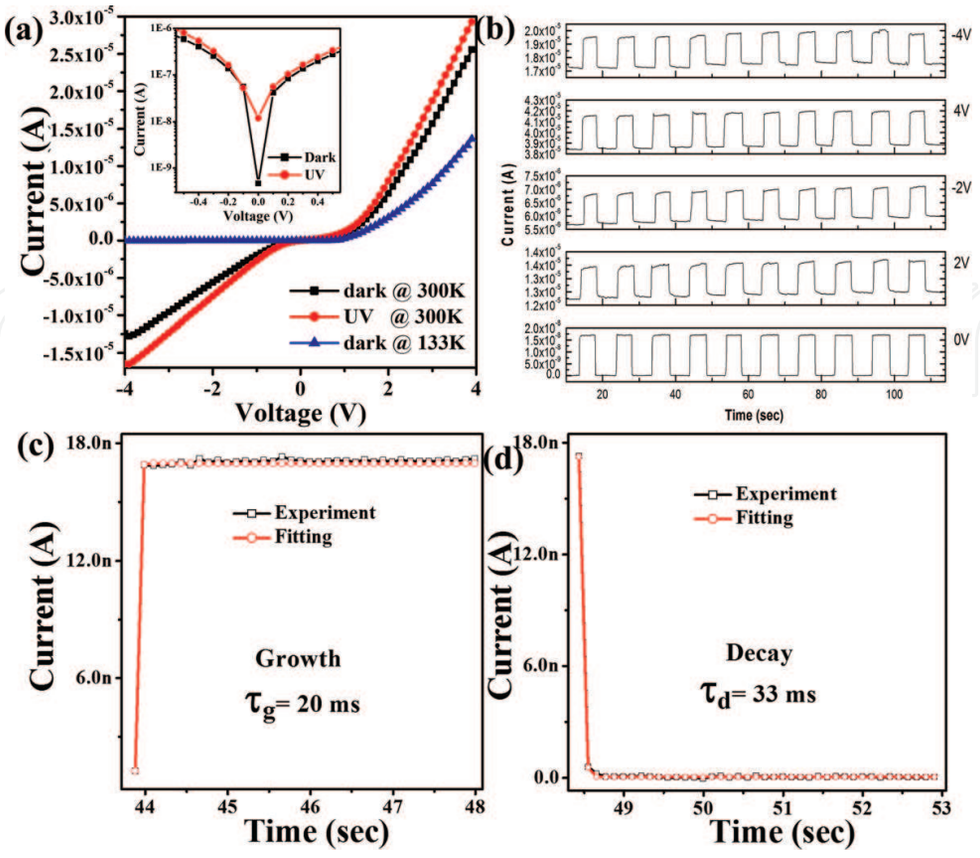

Figure 12. (a) Room temperature current-voltage characteristics of *n*-InGaN/*n*-Si heterojunction in dark at room temperature and at 133 K and under UV radiation at room temperature, (b) photoresponse at different working voltages, (c) time response of photocurrent growth, and (d) decay from the fitting of experimental values. Reprinted with permission from [88].

Voltage (V)	Responsivity (A/W)	EQE (%)
0	0.0942	32.4
2	0.6217	213.8
4	1.7097	588.1
−2	0.5746	197.6
−4	1.2575	432.5

Table 3. Bias-dependent responsivities and external quantum efficiencies.

range in each case is distinct from that of others, suggesting that such devices can be used for switching purposes and logical operations as well.

The mechanism for this type of behavior in n-n isotype heterojunctions can be explained with the help of a model proposed by Yawata et al. [77]. When the electron and hole pairs are generated, the electrons are swept away from the junctions due to the built-in electric field, whereas the holes are trapped in the notch. The holes being positively charged neutralize the electrons at interface and eventually lower the barrier height. For an intense illumination, the concentration of holes trapped at the notch is increased, thus drastically lowering the barrier

height and resulting in abrupt increase of electron flow. However, in case of a bias (positive or negative as explained above), the electrons at the interface tunnel through the depletion region leaving behind holes which are eventually refilled by electrons from the other side. The forward and negative bias characteristics from the current-voltage plots are in good agreement with the proposed mechanism.

5. Conclusions

In summary, we presented the studies on the growth, characterizations, and transport properties of III-nitride-based heterostructures. Here, discussion has been carried out on the growth of polar InN/GaN, nonpolar InN/GaN, polar InGaN/GaN, nonpolar InGaN/GaN, and InGaN/Si heterostructures by using MBE system followed by their characterizations. Moreover, we have presented the electrical transport properties across the heterostructures interface. In addition, UV and IR photodetection studies on InGaN/Si heterostructures have been discussed.

Author details

Basanta Roul[1,2], Greeshma Chandan[1], Shruti Mukundan[1] and Saluru Baba Krupanidhi[1]*

*Address all correspondence to: sbkenator@gmail.com

1 Materials Research Centre, Indian Institute of Science, Bangalore, India

2 Central Research Laboratory, Bharat Electronics, Bangalore, India

References

[1] Yoshida S, Misawa S, Gonda S. Improvements on the electrical and luminescent properties of reactive molecular beam epitaxially grown GaN films by using AlN-coated sapphire substrates. Applied Physics Letters. 1983;**42**:427

[2] Akasaki I, Amano H, Koide Y, Hiramatsu H, Sawak N. Effects of ain buffer layer on crystallographic structure and on electrical and optical properties of GaN and $Ga_{1-x}Al_xN$ ($0 < x \leqq 0.4$) films grown on sapphire substrate by MOVPE. Journal of Crystal Growth. 1989;**98**:209

[3] Nakamura S. GaN growth using GaN buffer layer. Japanese Journal of Applied Physics. 1991;**30**:L1705

[4] Nakamura S, Senoh M, Mukai T. P-GaN/N-InGaN/N-GaN double-heterostructure blue-light-emitting diodes. Japanese Journal of Applied Physics. 1993;**32**:L8-L11

[5] Nakamura S, Senoh M, Nagahama S, Iwasa N, Yamada T, Matsushita T, Kiyoku H, Sugimoto Y. InGaN-based multi-quantum-well-structure laser diodes. Japanese Journal of Applied Physics. 1996;**35**:L74

[6] Khan A, Kuzina MJN, Olson DT, Schaff WJ, Burm JW, Shur MS. Microwave performance of a 0.25 μm gate AlGaN/GaN heterostructure field effect transistor. Applied Physics Letters. 1994;**65**:1121-1122

[7] Waltereit P, Brandt O, Trampert A, Grahn HT, Menniger J, Ramsteiner M, Reiche M, Ploog KH. Nitride semiconductors free of electrostatic fields for efficient white light-emitting diodes. Nature. 2000;**406**:865

[8] Park SH, Ahn D. Depolarization effects in (11-22)-oriented InGaN/GaN quantum well structures Applied Physics Letters. 2007;**90**:013505

[9] Krames MR, Shchekin OB, Mueller-Mach R, Mueller GO, Zhou L, Harbers G, Craford MG. Status and future of high-power light-emitting diodes for solid-state lighting. Journal of Display Technology. 2007;**3**:160

[10] Sato H, Chung RB, Hirasawa H, Fellows, Masui H, Wu F, Saito M, Fujito K, Speck JS, DenBaars SP, Nakamura S. Optical properties of yellow light-emitting diodes grown on semipolar (11-22) bulk GaN substrates. Applied Physics Letters. 2008;**92**:221110

[11] Sun Q, Han J. Springer Series in Materials Science. 2012:156

[12] Craven MD, Wu F, Chakraborty A, Imer B, Mishra UK, DenBaars SP, Speck JS. Micro-structural evolution of *a*-plane GaN grown on *a*-plane SiC by metalorganic chemical vapor deposition. Applied Physics Letters. 2004;**84**:1281

[13] Sun Q, Yerino CD, Zhang Y, Cho YS, Kwon SY, Kong BH, Cho HK, Lee IH, Han J. Effect of NH_3 flow rate on *m*-plane GaN growth on m-plane SiC by metalorganic chemical vapor deposition. Journal of Crystal Growth. 2009;**311**:3824

[14] Trybus E. Molecular beam epitaxy growth of indium nitride and indium gallium nitride materials for photovoltaic applications [PhD thesis]. 2009

[15] Ambacher O, Smart J, Shealy JR, Weimann NG, Chu K, Murphy M, Schaff WJ, Eastman LF, Dimitrov R, Wittmer L, Stutzmann M, Rieger W, Hilsenbeck J. Two-dimensional electron gases induced by spontaneous and piezoelectric polarization charges in N- and Ga-face AlGaN/GaN heterostructures. Journal of Applied Physics. 1999;**85**:3222

[16] Khromov S. Doping effects on the structural and optical properties of GaN [PhD thesis]. 2013

[17] Monemar B, Pozina G. Group III-nitride based hetero and quantum structures. Progress in Quantum Electronics. 2000;**24**:239

[18] Shen YC, Mueller GO, Watanabe S, Gardner NF, Munkholm A, Krames MR. Auger recombination in InGaN measured by photoluminescence. Applied Physics Letters. 2007;**91**:141101

[19] Romanov AE, Young EC, Wu F, Tyagi A, Gallinat CS, Nakamura S, DenBaars SP, Speck JS. Basal plane misfit dislocations and stress relaxation in III-nitride semipolar heteroepitaxy. Journal of Applied Physics. 2011;**109**:103522

[20] Nye JF. Physical Properties of Crystals. New York: Oxford University Press; 1985

[21] Sano M, Aoki M, Epitaxial growth of undoped and Mg-doped GaN. Japanese Journal of Applied Physics. 1976;**15**:1943

[22] Madar R, Michel D, et al. Growth anisotropy in the GaN/Al2O3 system. Journal of Crystal Growth. 1977;**40**:239

[23] Craven MD, Lim SH, et al. Structural characterization of nonpolar (11-20) *a*-plane GaN thin films grown on (1-102) *r*-plane sapphire. Applied Physics Letters. 2002;**81**:469

[24] Kehagias T, Iliopoulos E, Delimitis A, Nouet G, Dimakis E, Georgakilas A, Komninou P. Interfacial structure of MBE grown InN on GaN. Physica Status Solidi (a). 2005; **202**:777

[25] Von Pezold J, Bristowe PD. Atomic structure and electronic properties of the GaN/ZnO (0001) interface. Journal of Material Science. 2005;**40**:3051

[26] Bernardini F, Fiorentini V. Macroscopic polarization and band offsets at nitride heterojunctions. Physical Review B. 1998;**57**:R9427

[27] Yoshikawa A, Che SB, YamaguchiW, Saito H,Wang XQ, Ishitani Y, Hwang ES. Proposal and achievement of novel structure InN/GaN multiple quantum wells consisting of 1 ML and fractional monolayer InN wells inserted in GaN matrix. Applied Physics Letters. 2007;**90**:073101

[28] Che SB, Terashima W, Ohkubo T, Yoshitani M, Hashimoto N, Akasaka K, Ishitani Y, Yoshikawa A. InN/GaN SQW and DH structures grown by radio frequency plasma-assisted MBE. Physica Status Solidi (c). 2005;**2**:2258

[29] Roul B, Kumar M, Rajpalke MK, Bhat TN, Kalghatgi AT, Krupanidhi SB. Effect of carrier concentration of InN on the transport behavior of InN/GaN heterostructure based Schottky junctions. Solid State Communication. 2012;**152**:1771

[30] Lin JC, Su YK, Chang SJ, Lan WH, Chen WR, Cheng YC, Lin WJ, Tzeng YC, Shin HY, Chang CM. InN grown on GaN/sapphire templates at different temperatures by MOCVD. Optical Materials. 2007;**30**:517

[31] Wu J. When group-III nitrides go infrared: New properties and perspectives. Journal of Applied Physics. 2009;**106**:011101

[32] Ponce FA, Bour DP. Nitride-based semiconductors for blue and green light-emitting devices. Nature. 1997;**386**:351

[33] Simeonov D, Feltin E, Buhlmann HJ, Zhu T, Castiglia A, Mosca M, Carlin JF, Butté R, Grandjean N. Blue lasing at room temperature in high quality factor GaN/AlInN microdisks with InGaN quantum wells. Applied Physics Letters. 2007;**90**:061106

[34] Rajpalke MK, Bhat TN, Roul B, Kumar M, Misra P, Kukreja LM, Sinha N, Krupanidhi SB. Growth temperature induced effects in non-polar *a*-plane GaN on *r*-plane sapphire substrate by RF-MBE. Journal of Crystal Growth. 2011;**314**:5

[35] Rajpalke MK, Roul B, Kumar M, Bhat TN, Sinha N, Krupanidhi SB. Structural and optical properties of nonpolar (11–20) *a*-plane GaN grown on (1–102) *r*-plane sapphire substrate by plasma-assisted molecular beam epitaxy. Scripta Materials. 2011;**65**:33

[36] Lu H, Schaff WJ, Eastman LF, Wu J, Walukiewicz W, Cimalla V, Ambacher O. Growth of *a*-plane InN on *r*-plane sapphire with a GaN buffer by molecular-beam epitaxy. Applied Physics Letters. 2003;**83**:1136

[37] Grandal J, Sánchez-García MA, Calleja E, Gallardo E, Calleja JM, Luna E, Trampert A, Jahn A. InN nanocolumns grown by plasma-assisted molecular beam epitaxy on AA-plane GaN templates. Applied Physics Letters. 2009;**94**:221908

[38] Cimalla V, Pezoldt J, Ecke G, Kosiba R, Ambacher O, Spiess L, Teichert G, Lu H, Schaff WJ. Growth of cubic InN on rr-plane sapphire. Applied Physics Letters. 2003;**83**:3468

[39] Tsuyuguchi A, Teraki K, Koizumi T, Wada J, Araki T, Nanishi Y, Naoi H. Institute of Physics Conference Series. 2005;**184**:239

[40] Weber ZL, Lu H, Schaff WJ, Kryliouk O, Park HJ, Mangum J, Anderson T. Comparison of structural perfection of InN layers and InN nanorods grown on the c- and r-planes of Al_2O_3. Physica Status Solidi (c). 2007;**4**:2469

[41] Ajagunna AO, Iliopoulos E, Tsiakatouras G, Tsagaraki K, Androulidaki M, Georgakilas A. Epitaxial growth, electrical and optical properties of a-plane InN on r-plane sapphire. Journal of Applied Physics. 2010;**107**:024506

[42] Rajpalke MK, Roul B, Bhat TN, Kumar M, Sinha N, Jali VM, Krupanidhi SB. Effects of growth temperature on nonpolar a-plane InN grown by molecular beam epitaxy. Physica Status Solidi (c). 2014;**11**:932

[43] Rajpalke MK, Bhat TN, Roul B, Kumar M, Krupanidhi SB. Current transport in nonpolar a-plane InN/GaN heterostructures Schottky junction. Journal of Applied Physics. 2012;**112**:023706

[44] Schuber R, Chou MMC, Vincze P, Schimmel Th, Schaadt DM. Growth of *A*-plane GaN on (0 1 0) $LiGaO_2$ by plasma-assisted MBE. Journal of Crystal Growth. 2010;**312**:1665

[45] Darakchieva V, Xie MY, Franco N, Giuliani F, Nunes B, Alves E, Hsiao CL, Chen LC, Yamaguchi T, Takagi Y, Kawashima K, Nanishi Y. Structural anisotropy of nonpolar and semipolar InN epitaxial layers. Journal of Applied Physics. 2010;**108**:073529

[46] Wu J,WalukiewiczW, ShanW, Yu KM, Ager JW III, Haller EE, Lu H, Schaff WJ. Effects of the narrow band gap on the properties of InN. Physical Review B. 2002;**66**:201403

[47] Zhang PF, Liu XL, Zhang RQ, Fan HB, Song HP, Wei HY, Jiao CM, Yang SY, Zhu QS, Wang ZG. Valence band offset of MgO/InN heterojunction measured by X-ray photoelectron spectroscopy. Applied Physics Letters. 2008;**92**:042906

[48] Nakamura S, Senoh M, Iwasa N, Nagahama S. High-power InGaN single-quantum-well-structure blue and violet light-emitting diodes. Applied Physics Letters. 1995;**67**:1868

[49] Laboutin O, Cao Y, Johnson W, Wang R, Li G, Jena D, Xing H. InGaN channel high electron mobility transistor structures grown by metal organic chemical vapor deposition. Applied Physics Letters. 2012;**100**:121909

[50] Hasan T, Kaysir R, Islam S, Bhuiyan AG, Islam R, Hashimoto A, Yamamoto A. 2DEG properties in InGaN/InN/InGaN-based double channel HEMTs. Physica Status Solidi (c). 2010;**7**:1997

[51] Sang L, Liao M, Koide Y, Sumiya M. High-temperature ultraviolet detection based on InGaN Schottky photodiodes. Applied Physics Letters. 2011;**99**:031115

[52] Cheong MG, Suh EK, Lee HJ, Dawson M. Growth and properties of InGaN/GaN quantum wells and blue light emitting diodes by metal–organic chemical vapour deposition. Semiconductor Science and Technology. 2002;**17**:446

[53] Kim IH, Park HS, Park YJ, Kim T. Formation of V-shaped pits in InGaN/GaN multiquantum wells and bulk InGaN films. Applied Physics Letters. 1998;**73**:1634

[54] Görgensa L, Ambacher O, Stutzmann M, Miskys C, Scholz F, Off J. Characterization of InGaN thin films using high-resolution X-ray diffraction. Applied Physics Letters. 2000;**76**:577

[55] Cao XA, Topol K, Sandvik FS, Teetsov FS, Sandvik PM, LeBoeuf SF, Ebong A, Kretchmer J, Stokes EB, Arthur S, Keloyeros AE, Walker D. Influence of defects on electrical and optical characteristics of GaN/InGaN-based light-emitting diodes. Proceedings of SPIE. 2002;**4776**:105

[56] Kim J, Cho YH, Ko DS, Li XS, Won JY, Lee E, Park SH, Kim JY, Kim S. Influence of V-pits on the efficiency droop in InGaN/GaN quantum wells. Optics Express.2014;**22**:A857

[57] Sinha N, Roul B, Mukundan S, Chandan G, Mohan L, Jali VM, Krupanidhi SB. Growth and electrical transport properties of InGaN/GaN heterostructures grown by PAMBE. Materials Research Bulletin. 2014;**61**:539-543

[58] El-Masry NA, Piner EL, Liu SX, Bedair SM. Phase separation in InGaN grown by metalorganic chemical vapor deposition. Applied Physics Letters. 1998;**72**:40

[59] Singh R, Doppalapudi D, Moustakas TD, Romano LT. Phase separation in InGaN thick films and formation of InGaN/GaN double heterostructures in the entire alloy composition. Applied Physics Letters.1997;**70**:1089

[60] Jmerik VN, Mizerov AM, Shubina TV, Yagovkina M, Listoshin VB, Sitnikova AA, Ivanov SV, Kim MH, Koike M, Kim BJ.Plasma-assisted MBE of InGaN epilayers with atomically smooth and nanocolumnar morphology, grown on MOVPE GaN/Al_2O_3 templates Journal of Crystal Growth. 2007;**3–302**:469

[61] Wang H, Jiang DS, Jahn U, Zhu JJ, Zhao DG, Liu ZS, Zhang SM, Qiu YX, Yang H. Investigation on the strain relaxation of InGaN layer and its effects on the InGaN structural and optical properties. Physica B. 2010;**405**:4668

[62] Chang YL, Wang JL, Li F, Mi Z. High efficiency green, yellow, and amber emission from InGaN/GaN dot-in-a-wire heterostructures on Si(111). Applied Physics Letters. 2010;**96**:013106

[63] Kehagias T, Dimitrakopulos GP, Becker P, Kioseoglou J, Furtmayr F, Koukoula T, Hausler I, Chernikov A, Chatterjee S, Karakostas T, Solowan HM, Schwarz UT, Eickhoff M, Komninou P. Nanostructure and strain in InGaN/GaN superlattices grown in GaN nanowires. Nanotechnology. 2013;**24**:435702

[64] Powell RC, Lee NE, Greene JE. Growth of GaN(0001)1×1 on Al_2O_3(0001) by gas-source molecular beam epitaxy. Applied Physics Letters. 1992;**60**:2505

[65] Pantha BN, Dahal R, Li J, Lin JY, Jiang HX, Pomrenke G. Thermoelectric properties of $In_xGa_{1-x}N$ alloys. Applied Physics Letters. 2008;**92**:042112

[66] McLaughlin DVP, Pearce JM. Progress in indium gallium nitride materials for solar photovoltaic energy conversion. Metallurgical and Materials Transactions A. 2013;**44**:1947

[67] Junqiao W. When group-III nitrides go infrared: New properties and perspectives. Journal of Applied Physics. 2009;**106**:011101

[68] Karpov SYu. Suppression of phase separation in InGaN due to elastic strain. MRS Internet Journal of Nitride Semiconductor Research. 1988;**3**:e16

[69] Keller S, Keller BP, Kapolnek D, Abare AC, Masui H, Coldren LA, Mishra UK, DenBaars SP. Growth and characterization of bulk InGaN films and quantum wells. Applied Physics Letters. 1996;**68**:3147

[70] Keller S, Keller BP, Kapolnek D, DenBaars SP, Shmagin IK, Kolbas RM, Krishnankutty S. Growth of bulk InGaN films and quantum wells by atmospheric pressure metalorganic chemical vapour deposition. Journal of Crystal Growth. 1997;**170**:349

[71] Song KM, Kim JM, Shin CS, Hwangand Dae SM, Yoon H. Growth and characterization of *a*-plane InGaN/GaN multiple quantum well LEDs grown on r-plane sapphire. Semiconductors and Science Technology. 2012;**27**:015011

[72] Paskova T, Kroeger R, Figge S, Hommel D, Darakchieva V, Monemar B, Preble E, Hanser A, Williams NM, Tutor M. High-quality bulk a-plane GaN sliced from boules in comparison to heteroepitaxially grown thick films on r-plane sapphire. Applied Physics Letters. 2006;**89**:051914

[73] Heying B,Wu XH, Keller S, Li Y, Kapolnek D, Keller BP, DenBaars SP, Speck JS. Role of threading dislocation structure on the x-ray diffraction peak widths in epitaxial GaN films. Applied Physics Letters. 1996;**68**:643

[74] Chierchia R, Bottcher T, Figge S, Diesselberg M, Heinke H, Hommel D. Mosaicity of GaN epitaxial layers: Simulation and experiment. Physica Status Solidi (b). 2001;**228**:403

[75] Wang H, Chen C, Gong Z, Zhang J, Gaevski M, Su M, Yang J, Asif Kahn M. Anisotropic structural characteristics of (1120) GaN templates and coalesced epitaxial lateral overgrown films deposited on (1012) sapphire. Applied Physics Letters. 2004;**84**:499

[76] Kim HY, Kim JH, Kim YJ, Chae KH, Whang CN, Song JH, Im S. Photoresponse of Si detector based on n-ZnO/p-Si and n-ZnO/n-Si structures. Optical Materials. 2001;**17**:141

[77] Yawata S, Anderson RL. Optical modulation of current in Ge-Si N-N heterojunctions. Physica Status Solidi. 1965;**12**:297

[78] Tan ST, Sun XW, Zhao JL, Iwan S, Cen ZH, Chen TP, Ye JD, Lo GQ, Kwong DL, Teo KL. Ultraviolet and visible electroluminescence from n-ZnO/SiO_x/(n,p)-Si heterostructured light-emitting diodes. Applied Physics Letters. 2008;**93**:013506

[79] Hudait MK, Krupanidhi SB. Growth, optical, and electron transport studies across isotype n-GaAs/n-Ge heterojunctions. Journal of Vacuum Science & Technology B: Microelectronics and Nanometer Structures. 1999;**17**:1003

[80] Milnes AG. Semiconductor Heterojunction Topics—Introduction and Overview. Solid-State Electronics. 1986;**29**:99

[81] Tansley TL, Owen SJT. Conductivity of Si-ZnO p-n and n-n heterojunctions. Journal of Applied Physics. 1984;**55**:454

[82] Srivastava AK, Zyskind JL, Lum RM, Dutt BV, Klingert JK. Electrical characteristics of InAsSb/GaSb heterojunctions. Applied Physics Letters.1986;**49**:41

[83] Ager JW, Reichertz LA, Cui Y, Romanyuk YE, Kreier D, Leone SR, Man K, Yu M, Schaff WJ, Walukiewicz W. Electrical properties of InGaN-Si heterojunctions. Physica Status Solidi (c). 2009;**6**(S2):S413

[84] Kumar P, Soto Rodriguez PED, Gómez VJ, Alvi NH, Calleja E, Nötzel R. First demonstration of direct growth of planar high-in-composition InGaN layers on Si. Applied Physics Express. 2013;**6**:035501

[85] Hatch SM, Briscoe J, Dunn S. A self-powered ZnO-nanorod/CuSCN UV photodetector exhibiting rapid response. Advanced Materials. 2013;**25**:867

[86] Bie YQ, Liao ZM, Zhang HZ, Li GR, Ye Y, Zhou YB, Xu J, Qin ZX, Dai L, Yu DP. Self-powered, ultrafast, visible-blind UV detection and optical logical operation based on ZnO/GaN nanoscale p-n junctions. Advanced Materials. 2011;**23**:649

[87] Ohsawa J, Kozawa T, Fujishima O, Itoh H. Narrow-band 400 nm MSM photodetectors using a thin InGaN layer on a GaN/sapphire structure. Physica Status Solidi (c). 2006;**3**:2278

[88] Chandan G, Mukundan S, Mohan L, Roul B, Krupanidhi SB. Trap modulated photoresponse of InGaN/Si isotype heterojunction at zero-bias. Journal of Applied Physics. 2015;**118**:024503

[89] Orsal G, El Gmili Y, Fressengeas N, Streque J, Djerboub R, Moudakir T, Sundaram T, Ougazzaden A, Salvestrini JP. Bandgap energy bowing parameter of strained and relaxed InGaN layers. Optical Materials Express. 2014;**4**:1030

[90] Wu J, Walukiewicz W, Yu KM, Ager JW, Haller EE, Lu H, Schaff WJ. Small band gap bowing in $In_{1-x}Ga_xN$ alloys. Applied Physics Letters. 2002;**80**:4741

[91] Reklaitis A. Terahertz-frequency InN/GaN heterostructure-barrier varactor diodes. Journal of Physics: Condensed Matter. 2008;**20**:384202

[92] Tsen KT, Poweleit C, Ferry DK, Lu H, Schaff WJ. Observation of large electron drift velocities in InN by ultrafast Raman spectroscopy. Applied Physics Letters. 2005;**86**:222103

[93] Chen NC, Chang PH, Wang YN, Peng HC, Lien WC, Shih CF, Chang CA, Wu GM. Schottky behavior at InN–GaN interface. Applied Physics Letters. 2005;**87**:212111

[94] Wang K, Lian C, Su. N, Jena D, Timler J. Conduction band offset at the InN◎GaN heterojunction. Applied Physics Letters. 2007;**91**:232117

[95] Roul B, Rajpalke MK, Bhat TN, Kumar M, Sinha N, Kalghatgi AT, Krupanidhi SB. Temperature dependent electrical transport behavior of InN/GaN heterostructure based Schottky diodes. Journal of Applied Physics. 2011;**109**:044502

[96] Roul B, Kumar M, Rajpalke MK, Bhat TN, Krupanidhi SB. Binary group III-nitride based heterostructures: band offsets and transport properties. Journal of Physics D: Applied Physics. 2015;**48**:423001

[97] Tung RT. Recent advances in Schottky barrier concepts. Material Science Engineering R. 2001;**35**:1

[98] Hattab A, Perrossier JL, Meyer F, Barthula M, Osten HJ, Griesche J. Schottky barrier inhomogeneities at contacts to carbon-containing silicon/germanium alloys. Material Science Engineering B. 2002;**89**:284

[99] Cimilli FE, Saglam M, Turut A. Determination of the lateral barrier height of inhomogeneous Au/n-type InP/In Schottky barrier diodes. Semiconductors and Science Technology. 2007;**22**:851

[100] Singh A. Characterization of interface states at Ni/*n*CdF2 Schottky barrier type diodes and the effect of CdF_2 surface preparation. Solid-State Electronics. 1985;**28**:223

[101] McCafferty PG, Sellai A, Dawson P, Elabd H. Barrier characteristics of PtSi/p-Si schottky diodes as determined from I-V-T measurements. Solid-State Electronics. 1996;**39**:583

[102] Roul B, Bhat TN, Kumar M, Rajpalke MK, Sinha N, Kalghatgi AT, Krupanidhi SB. Barrier height inhomogeneities in InN/GaN heterostructure based Schottky junctions. Solid State Communication. 2011;**151**:1420

[103] Arslan E, Altındal S, Ozcelik S, Ozbay E. Tunneling current via dislocations in Schottky diodes on AlInN/AlN/GaN heterostructures. Semiconductors and Science Technology. 2009;**24**:075003

[104] Roul B, Mukundan S, Chandan G, Mohan L, Krupanidhi SB. Barrier height inhomogeneity in electrical transport characteristics of InGaN/GaN heterostructure interfaces. AIP Advances. 2015;**5**:037130

[105] Milnes AG, Oldham WG. Semiconductor heterojunction topics—Introduction and overview. Solid State Electronics. 1963;**6**:121

[106] Pantha BN, Wang H, Khan N, Lin JY, Jiang HX. Origin of background electron concentration in $In_xGa_{1-x}N$ alloys. Physical Review B. 2011;**84**:7

[107] Ghosh S, Sarker BK, Chunder A, Zhai L, Khondaker SI. Position dependent photodetector from large area reduced graphene oxide thin films. Applied Physics Letters. 2010; **96**:163109

[108] Chitara B, Krupanidhi SB, Rao CNR. Solution processed reduced graphene oxide ultraviolet detector. Applied Physics Letters. 2011;**99**:113114

IntechOpen